Published June 15, 2009



# Formation of cristae and crista junctions in mitochondria depends on antagonism between Fcj1 and Su *e*/*g*

Regina Rabl,[1,2] Vincent Soubannier,[1,2,3] Roland Scholz,[4] Frank Vogel,[5] Nadine Mendl,[1,2] Andreja Vasiljev-Neumeyer,[1,2] Christian Körner,[1,2] Ravi Jagasia,[6] Thomas Keil,[4] Wolfgang Baumeister,[4] Marek Cyrklaff,[4] Walter Neupert,[1,2,4] and Andreas S. Reichert[1,2,7]

[1]Adolf-Butenandt Institute for Physiological Chemistry, and [2]Center for Integrated Protein Science Munich, Ludwig-Maximilians University, 81377 Munich, Germany
[3]University of Ottawa Heart Institute, Ottawa, Ontario K1Y 4W7, Canada
[4]Max-Planck-Institut für Biochemie, 82152 Martinsried, Germany
[5]Max-Delbrück-Centrum für molekulare Medizin Berlin-Buch, 13092 Berlin, Germany
[6]Institute of Developmental Genetics, Hemholtz Center Munich, German Research Center for Environmental Health, GmbH, 85764 Neuherberg, Germany
[7]Mitochondrial Biology, Cluster of Excellence Frankfurt Macromolecular Complexes, Johann Wolfgang Goethe University Medical School, 60590 Frankfurt am Main, Germany

Crista junctions (CJs) are important for mitochondrial organization and function, but the molecular basis of their formation and architecture is obscure. We have identified and characterized a mitochondrial membrane protein in yeast, Fcj1 (formation of CJ protein 1), which is specifically enriched in CJs. Cells lacking Fcj1 lack CJs, exhibit concentric stacks of inner membrane in the mitochondrial matrix, and show increased levels of $F_1F_O$–ATP synthase ($F_1F_O$) supercomplexes. Overexpression of Fcj1 leads to increased CJ formation, branching of cristae, enlargement of CJ diameter, and reduced levels of $F_1F_O$ supercomplexes. Impairment of $F_1F_O$ oligomer formation by deletion of its subunits *e*/*g* (Su *e*/*g*) causes CJ diameter enlargement and reduction of cristae tip numbers and promotes cristae branching. Fcj1 and Su *e*/*g* genetically interact. We propose a model in which the antagonism between Fcj1 and Su *e*/*g* locally modulates the $F_1F_O$ oligomeric state, thereby controlling membrane curvature of cristae to generate CJs and cristae tips.

## Introduction

Mitochondria are ubiquitous organelles and fulfill a multitude of crucial functions in eukaryotic organisms. Mitochondria are made up by two membranes: the outer membrane (OM) and the inner membrane (IM). The IM is composed of two subdomains: the inner boundary membrane (IBM) and the cristae membrane (CM). The IBM is closely apposed to the OM, both forming a double-layered envelope of the organelle. CMs are invaginations of the IBM that protrude into the matrix space. Large variations exist in the morphology of CMs (Munn, 1974; Fawcett, 1981; for review see Zick et al., 2009), and aberrant mitochondrial structures have been described for numerous pathological situations in humans (DiMauro et al., 1985; Wallace, 2005). Tubular-, lamellar-, and even triangle-shaped structures of the CM have been observed (Fawcett, 1981). Cristae are connected to the IBM by narrow tubular- or slotlike structures of varying length, so-called crista junctions (CJs), as revealed by EM of serial sections of mitochondria (Daems and Wisse, 1966) and by electron tomography (Mannella et al., 1994; Perkins et al., 1997, 1998; Nicastro et al., 2000; Frey et al., 2002; for reviews see Frey and Mannella, 2000; Mannella et al., 2001). The diameter of CJs was found to be rather small, ranging from 12 to 40 nm (Nicastro et al., 2000; Perkins et al., 2003; for review see Frey and Mannella, 2000). This led to the suggestion of CJs forming barriers for the movement of proteins and metabolites between the intracristal and the intermembrane space as well as

R. Rabl and V. Soubannier contributed equally to this paper.

Correspondence to Andreas S. Reichert: reichert@zbc.kgu.de

Abbreviations used in this paper: BN-PAGE, blue native PAGE; CJ, crista junction; CM, cristae membrane; DIC, differential interference contrast; IBM, inner boundary membrane; IM, inner membrane; mtDNA, mitochondrial DNA; OM, outer membrane; PK, proteinase K; SEC, size exclusion chromatography; TAP, tandem affinity purification.



The Rockefeller University Press $30.00
J. Cell Biol. Vol. 185 No. 6 1047–1063
www.jcb.org/cgi/doi/10.1083/jcb.200811099

Supplemental Material can be found at:
http://jcb.rupress.org/cgi/content/full/jcb.200811099/DC1

Published June 15, 2009

between the CM and the IBM (Mannella et al., 1994). Such a role of CJs has been proposed to have important consequences for the regulation of oxidative phosphorylation, as a barrier of this kind might limit the diffusion of metabolites like ADP into the intracristal space and modulate the pH gradient across the IM (Perkins et al., 1997; Renken et al., 2002; for reviews see Mannella et al., 2001; Mannella, 2006a). Also, subcompartmentalization of the IM was suggested based on biochemical subfractionation of mitochondria (Werner and Neupert, 1972; Pon et al., 1989), localization of individual mitochondrial proteins by immuno-EM (Gilkerson et al., 2003), or fluorescence microscopy (Wurm and Jakobs, 2006). Recently, this subcompartmentalization was addressed by determining the distribution of 20 mitochondrial proteins using quantitative immuno-EM (Vogel et al., 2006). The IBM appears to be segregated from the CM by the CJ, yet proteins are able to dynamically redistribute between the two subcompartments of the IM depending on the physiological state of the cell (Vogel et al., 2006). Furthermore, CJs undergo remodeling during apoptosis; this was suggested to allow release of the intracristal pool of cytochrome *c* to the cytoplasm, thereby triggering programmed cell death (Scorrano et al., 2002; Cipolat et al., 2006; Frezza et al., 2006).

Despite the apparent importance of the structural organization of mitochondria, the components responsible for the morphology and biogenesis of cristae, and in particular of CJs, are largely unknown. Deletion of the dimer-specific subunit *e* (Su *e*) or Su *g* of the $F_1F_O$–ATP synthase ($F_1F_O$) leads to defective oligomerization of this complex (Arnold et al., 1998) and to altered cristae morphology with extended onion-like structures in yeast (Paumard et al., 2002). Furthermore, remodeling of CJs during apoptosis was reported to depend on the mitochondrial dynamin-like protein OPA1 (Frezza et al., 2006). Prohibitins were recently suggested to play a role in cristae morphogenesis by controlling OPA1 processing (Merkwirth et al., 2008). The yeast orthologue of OPA1, Mgm1, was proposed to be required for cristae maintenance in addition to its role in IM fusion (Wong et al., 2003; Meeusen et al., 2006). Another protein reported to determine cristae morphology in human cells is mitofilin. Downregulation of this protein led to massive proliferation of the IM, resulting in multiple layers that appear to be interconnected accompanied by a disappearance of CJs (John et al., 2005). Mitofilin was initially named heart muscle protein, as it is highly expressed in rat heart tissue (Icho et al., 1994). Proteomic analysis of human heart mitochondria further indicated high abundance of this protein in mitochondria (Taylor et al., 2003). The name mitofilin was coined because of its colocalization with filament-like mitochondria in fibroblasts (Odgren et al., 1996).

In summary, a few proteins are known to influence cristae morphology, but, so far, no protein has been shown to be specifically localized to CJs or to be part of a CJ protein complex. In this study, we investigated the molecular basis governing the architecture of cristae and CJs in mitochondria of the yeast *Saccharomyces cerevisiae*. We describe ultrastructural alterations of the IM of yeast mitochondria lacking the open reading frame *AIM28* (*YKR016w/FMP13*) with hitherto unknown function. This gene was recently listed as a putative orthologue of mammalian mitofilin (Olichon et al., 2006). We provide both morphological and biochemical evidence that this protein is directly involved in the formation and molecular structure of CJs and is specifically enriched at CJs. We propose to name it Fcj1 (formation of CJ protein 1). Fcj1 regulates the oligomeric state of the $F_1F_O$ supercomplex in an adverse manner, and, moreover, CJ formation and structure turn out to be dependent on $F_1F_O$ supercomplex formation itself. Furthermore, Su *e* and Su *g* of $F_1F_O$, which promote oligomerization of $F_1F_O$, are essential for the formation of endings of cristae, the tips, or rims. The $F_1F_O$ complex has been proposed to represent a key element in the determination of cristae structure (Paumard et al., 2002), a proposal which rests on its very high abundance in the mitochondrial IM. In this study, we present a working model that explains the control of cristae architecture by the antagonistic effects of Fcj1 and $F_1F_O$ Su *e* and Su *g* on the oligomeric state of $F_1F_O$.

## Results

### Deletion of Fcj1 leads to altered mitochondrial morphology and partial loss of mitochondrial DNA (mtDNA)

In a search for genes affecting mitochondrial structure, we analyzed a collection of yeast cells that showed deficiency in growth on nonfermentable carbon sources because mutants with this phenotype are often accompanied by alterations in mitochondrial structure. We focused on genes coding for putative mitochondrial proteins that, so far, do not have an assigned function. Possible candidate strains were checked for mitochondrial morphology by rhodamine staining and then by expression of matrix-targeted GFP. We identified a mutant that showed alterations in the typical mitochondrial network. In the strain lacking the open reading frame *FCJ1* (*AIM28/FMP13/YKR016w*), abnormally large spherical mitochondria were observed. These were mostly located in the periphery of the cell and formed atypical networks (Fig. 1 A). In addition, mitochondria occasionally appeared hollow. For further characterization, we determined the percentage of $rho^0/rho^-$ cells. Depending on the cell density and the growth medium used, this value varied from 15 to 40% for the mutant cells. The respiratory rates of isolated mitochondria from such cells in state III (+ADP) and state IV (−ADP) and the maximal uncoupled rates were reduced by 30% as compared with wild type (Table I). The membrane potential, $\Delta\psi$, of the mutant mitochondria was also reduced compared with wild type, although to a lesser extent (Table I). The respiratory control ratio (state III/state IV rates) in the mutant was not altered, indicating that the respiratory chain and the ATP synthase were still well coupled. Taking all of these observations into account, compromised respiration in the mutant cells was rather caused by a secondary loss of mtDNA than by primary deficiencies of enzymatic activities involved in oxidative phosphorylation.

### Fcj1 is located in the mitochondrial IM facing the intermembrane space with its large hydrophilic domain

The *FCJ1* (*AIM28/FMP13/YKR016w*) gene encodes a protein of 540 aa residues. In silico analysis by the MitoProt II program (Claros and Vincens, 1996) yielded a high probability for

Published June 15, 2009

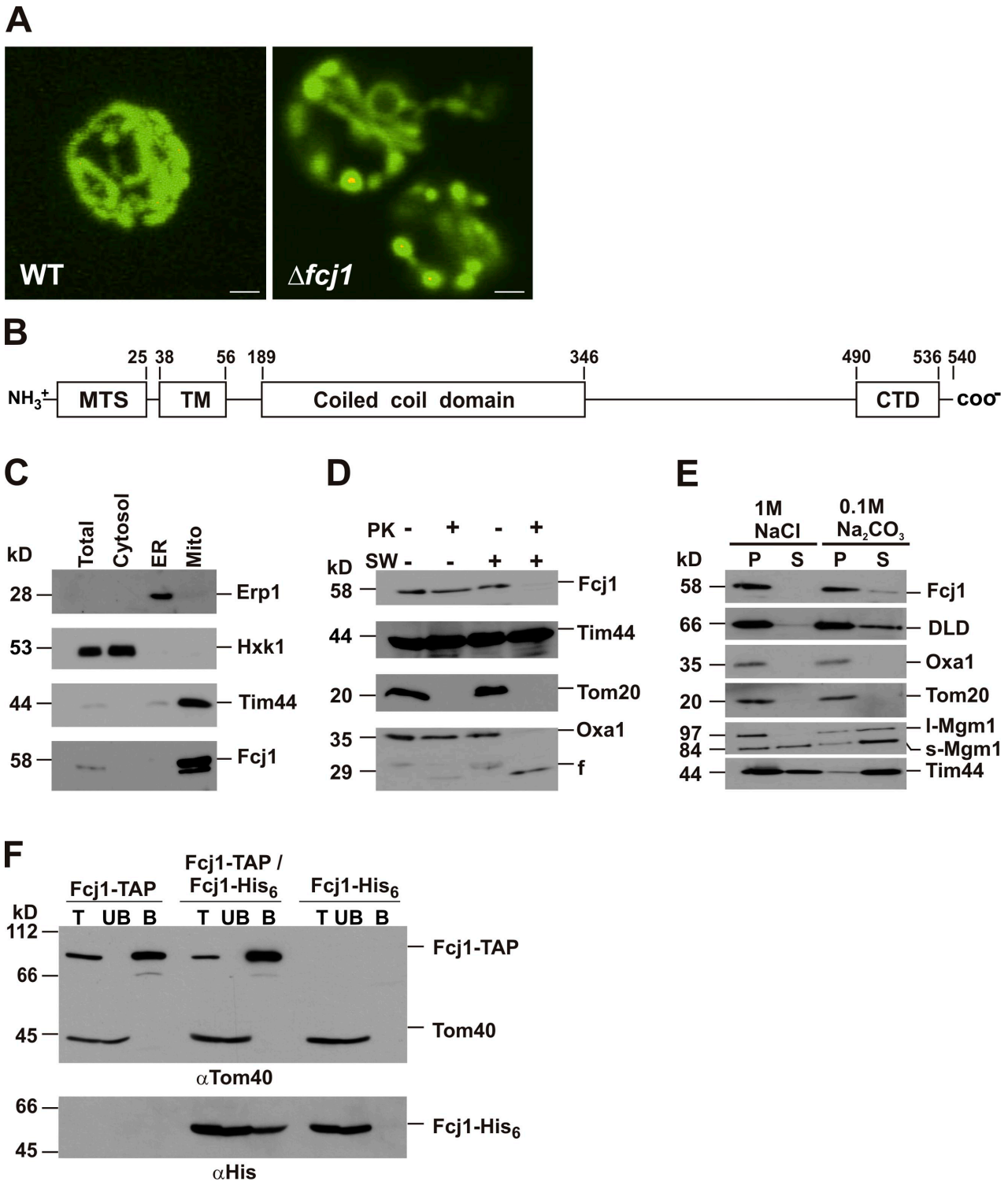


Figure 1. **Fcj1 is required for normal mitochondrial morphology.** (A) Wild-type (WT) and *Δfcj1* cells expressing mitochondria-targeted GFP were grown on nonfermentable medium and visualized by fluorescence microscopy. (B) Domain structure of Fcj1 depicting the mitochondrial-targeting sequence (MTS), the transmembrane segment (TM), the coiled-coiled domain, and the conserved C-terminal domain (CTD) with corresponding positions of amino acid residues. (C) Subcellular fractionation of wild-type cells: mitochondria (Mito), microsomes (ER), and cytosol. Equal amounts of protein (50 μg) were analyzed by Western blotting with the indicated marker proteins: Tim44 (Mito), Erp1 (ER), and Hxk1 (Cytosol). (D) Submitochondrial localization of Fcj1. Wild-type mitochondria and mitoplasts generated by hypotonic swelling (SW) were treated with PK. f, specific proteolytic fragment of Oxa1. (E) Membrane association of Fcj1. Wild-type mitochondria were extracted with NaCl or Na carbonate. Membrane-bound (P) and soluble (S) fractions were loaded and analyzed by Western blotting using the indicated marker proteins. DLD, D-lactate dehydrogenase. (F) Homotypic interaction of Fcj1. Mitochondria from cells expressing a His-tagged (Fcj1-$His_6$) or a TAP-tagged variant of Fcj1 (Fcj1-TAP) or both were subjected to TAP affinity chromatography. Total (T; 10%), bound (B; 100%), and unbound (UB; 10%) material was analyzed by Western blotting with the indicated antibodies. Tom40 and TAP-tagged Fcj1 were detected simultaneously using rabbit antibodies against Tom40. Bars, 1 μm.

Published June 15, 2009

Table I. **Bioenergetic characterization of wild-type and *Δfcj1* cells**

| Bioenergetic properties of isolated mitochondria | Wild type | *Δfcj1* |
|---|---|---|
| Uncoupled respiration (nmol oxygen/min/mg of protein) | 248.5 ± 41.27 (*n* = 3) | 174.6 ± 30.9 (*n* = 3)[a] |
| Respiratory control (state III/state IV) | 3.01 ± 0.23 (*n* = 3) | 2.93 ± 0.09 (*n* = 3) |
| Membrane potential ΔΨ (ΔF/F) | 0.285 ± 0.019 (*n* = 3) | 0.221 ± 0.032 (*n* = 3)[b] |
| ATPase activity (nmol $P_i$/min/mg of protein) | | |
| −oligomycin | 1,393 ± 231 (*n* = 3) | 1,264 ± 121 (*n* = 3)[c] |
| +oligomycin | 275 ± 93 (*n* = 3) | 256 ± 102 (*n* = 3)[d] |

F, fluorescence. For measuring bioenergetic properties, mitochondria were isolated from cells grown at 30°C on complete liquid media containing 2% (vol/vol) lactate. Mean values together with standard deviations (±) of *n* measurements are given.

[a]70% of wild type.

[b]78% of wild type.

[c]91% of wild type.

[d]93% of wild type.

mitochondrial targeting (0.9967), including a predicted cleavage site of the mitochondrial processing peptidase between positions 16 and 17 and a possible site of the mitochondrial intermediate peptidase between residues 24 and 25 (Fig. 1 B). Furthermore, Fcj1 contains a predicted single transmembrane segment close to the N terminus. Fcj1 shares 13% sequence identity with human mitofilin and 12% with mouse mitofilin. At the C terminus, it contains a short segment of higher similarity (Fig. S1). Several structural features such as the position of the transmembrane segment, a coiled-coil domain, and the conserved C-terminal domain argue for Fcj1 being a member of the mitofilin protein family.

Upon subcellular fractionation, Fcj1 was completely recovered in the mitochondria (Fig. 1 C). Incubation of isolated mitochondria with proteinase K (PK) did not lead to degradation of Fcj1; however, after selective opening of the OM, Fcj1 was degraded (Fig. 1 D). Treatment of mitochondria with either high salt or Na carbonate did not result in extraction of the protein (Fig. 1 E). To test whether Fcj1 can form oligomeric structures, two differently C-terminally tagged variants of Fcj1, a His-tagged (Fcj1-$His_6$) and a tandem affinity purification (TAP)–tagged variant (Fcj1-TAP), were coexpressed in yeast. Upon TAP affinity chromatography, Fcj1-$His_6$ was copurified with Fcj1-TAP, indicating that Fcj1 undergoes homotypic interactions (Fig. 1 F). Affinity purification of Fcj1-$His_{12}$ from *Δfcj1 + Fcj1-$His_{12}$* mitochondria solubilized in Triton X-100 did not lead to copurification of proteins other than Fcj1-$His_{12}$ (Fig. S2 A). The size of the Fcj1-$His_{12}$ complex in Triton X-100–solubilized mitochondria was ∼180 kD, as determined by size exclusion chromatography (SEC). Moreover, the complex retained its size after affinity purification, which is consistent with the formation of a stable homo-oligomeric complex (Fig. S2 B). The size would suggest a trimeric complex; however, a dimeric or tetrameric complex seems possible as well. We also analyzed the size of the Fcj1 complex after TAP from mitochondria harboring Fcj1-$His_6$ and Fcj1-TAP. The size of the Fcj1-TAP–Fcj1-$His_6$ complex was shifted to a molecular mass of ∼320 kD or ∼220 kD depending on the detection of the TAP tag or the His tag, respectively (Fig. S2 C). This increase in molecular mass is consistent with the presence of one or more subunits of Fcj1 containing the 20-kD TAP tag, further strengthening the view of a homo-oligomeric Fcj1 complex. Collectively, Fcj1 is a protein engaged in homotypic interactions that is anchored to the mitochondrial IM with its major part exposed to the intermembrane space.

### Fcj1 is enriched at CJs

We determined the distribution of Fcj1 over the various subdomains of the IM using quantitative immuno-EM. Cryosections of chemically fixed wild-type cells were immunodecorated with antibodies against Fcj1 and visualized by immunogold. Low concentrations of antibodies were used to keep the level of unspecific immunodecoration low. The specificity of the Fcj1 antibody was confirmed by Western blotting as well as by immunogold labeling of wild-type and *Δfcj1* cells (Fig. S3, A and B). Gold particles present in a large number of sections of wild-type cells were projected on a model, as described previously (Vogel et al., 2006), representing OM, IBM, CM, and a CJ (Fig. 2, A and B). Fcj1 was most prominently clustered in close proximity to the CJ (Fig. 2, A and B), a region which, so far, was rather characterized by a quite low density of numerous other mitochondrial proteins (for comparison see Vogel et al. [2006]). A region nearly lacking gold particles was observed in the CM adjacent to the CJ region (Fig. 2 B). This necklike region represents the narrow tubular segment of the CM, exhibiting a relatively high positive membrane curvature. The curvature here is opposite to the one at the base of CJs. Fcj1 was present to some extent in the remainder of the CM, including the cristae tips and in the IBM distant from the CJ region. The term cristae tip refers to its appearance in electron micrographs of mitochondrial sections. Depending on the section plane, they represent the highly positively curved rims of lamellar-like CM sheets. To evaluate these findings in a quantitative way, a sliding window was moved along the IM of our model starting from the bottom, counting only gold particles that were located within 14-nm distance from the IM (Fig. 2, C and D). This was performed for Fcj1 and as a control for Cox2, a subunit of cytochrome *c* oxidase, as well as for Su *e* and Su *g* of $F_1F_O$ (Fig. 2, C and D; raw data for Cox2 and Su *e* and Su *g* were taken from Vogel et al. [2006]). With Fcj1, the highest number of gold particles was observed in the region corresponding to the CJ (Fig. 2, C and D, gray boxes). The number of gold particles representing Cox2 was very low in the CJ and IBM region and increased in the CM (Fig. 2 C; Vogel et al., 2006). Su *e* and Su *g* of $F_1F_O$ were not enriched in the CJ region

Published June 15, 2009

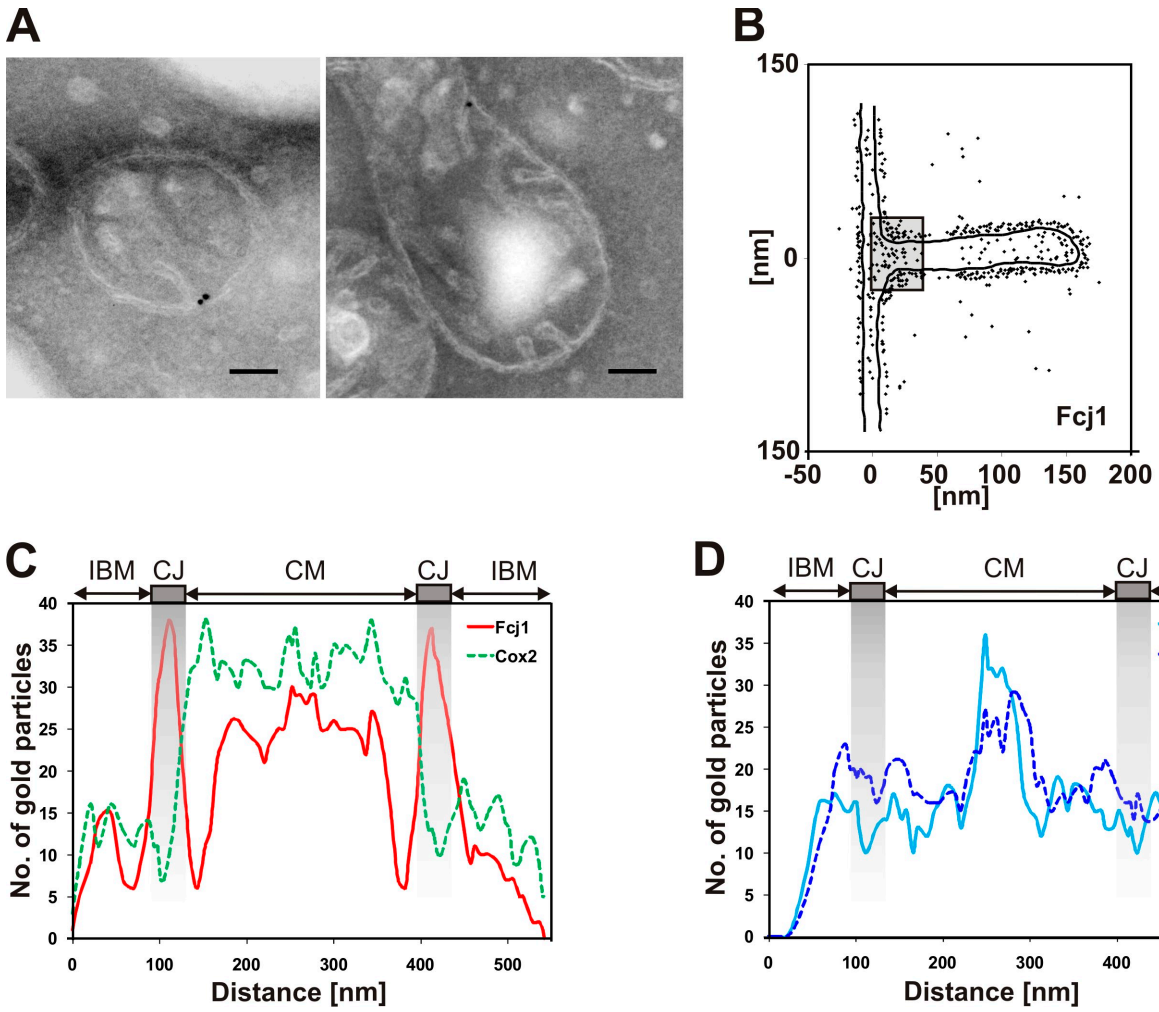


Figure 2. **Fcj1 is enriched at CJs.** (A) Immunogold labeling of Fcj1 in wild-type cells. (B) Representation of gold particles after immunogold labeling of Fcj1 plotted on a model of CM, IBM, and OM (Vogel et al., 2006). (C and D) Quantification of protein densities in the IM. The number of gold particles occurring within a 14-nm distance from the IM was determined by moving a sliding window in silico along the IM in the model from bottom to top (raw data from C and from Vogel et al. [2006]). Gray boxes indicate the CJ region. The protein densities of Fcj1 and Cox2 (C) and of Su *g* and Su *e* (D) are shown. Bars, 100 nm.



but rather appeared accumulated in the cristae tips (Fig. 2 D). Collectively, the enrichment of Fcj1 at CJs was unique and not observed for any of the proteins analyzed previously (Fig. 2, C and D; Vogel et al., 2006). The presence of Fcj1 in lower amounts in the planar parts of the cristae, where the levels of Su *e* and Su *g* are also intermediate, could reflect a balance of function in these regions; in part, they could also be caused by the topological complexity of bent cristae and perhaps, to a lesser degree, by background signals. Altogether, our data demonstrate that Fcj1 is the only protein identified so far specifically enriched at CJs at sites where the amounts of Su *e* and Su *g* are relatively low.

### Deletion of Fcj1 leads to loss of CJs and altered cristae morphology

The morphology of mitochondrial IMs was studied by EM and tomographic reconstruction from sections of yeast cells prepared by the Tokuyasu method (Tokuyasu, 1989). In wild-type cells, mitochondria showed a large number of CJs, and the IM and OM were often in very close proximity at the bases of CJs (Fig. 3, A and B; Table II; and Video 1). In *Δfcj1* cells, mitochondria were increased in size and contained numerous internal cristae with no apparent CJs (Fig. 3, C and D; Table II; and Video 2). These CMs were arranged mainly as parallel, concentric, stacked vesicular structures. The lumen of the vesicular structures was identified as intracristal space (Fig. S3 C). In a further approach, rapidly frozen hydrated spheroplasted yeast cells were subjected to cryosectioning and cryo-EM tomography. In addition, isolated mitochondria were analyzed by cryo-EM tomography. Both procedures led to high resolution structures of CJs in wild-type cells (Fig. 4, A and B; Fig. S4, A–C; and Video 3) and revealed the absence of CJs in *Δfcj1* mitochondria (Fig. 4 C, Fig. S4 D, and Video 4).

The narrow matrix space between adjacent CMs in mitochondria of *Δfcj1* cells contained particles of uniform size and shape that were arranged in a zipperlike pattern (Fig. 4, D–G; and Videos 4 and 5). Top views reveal the distribution and organization of these complexes as short linear assemblies or as two

Published June 15, 2009

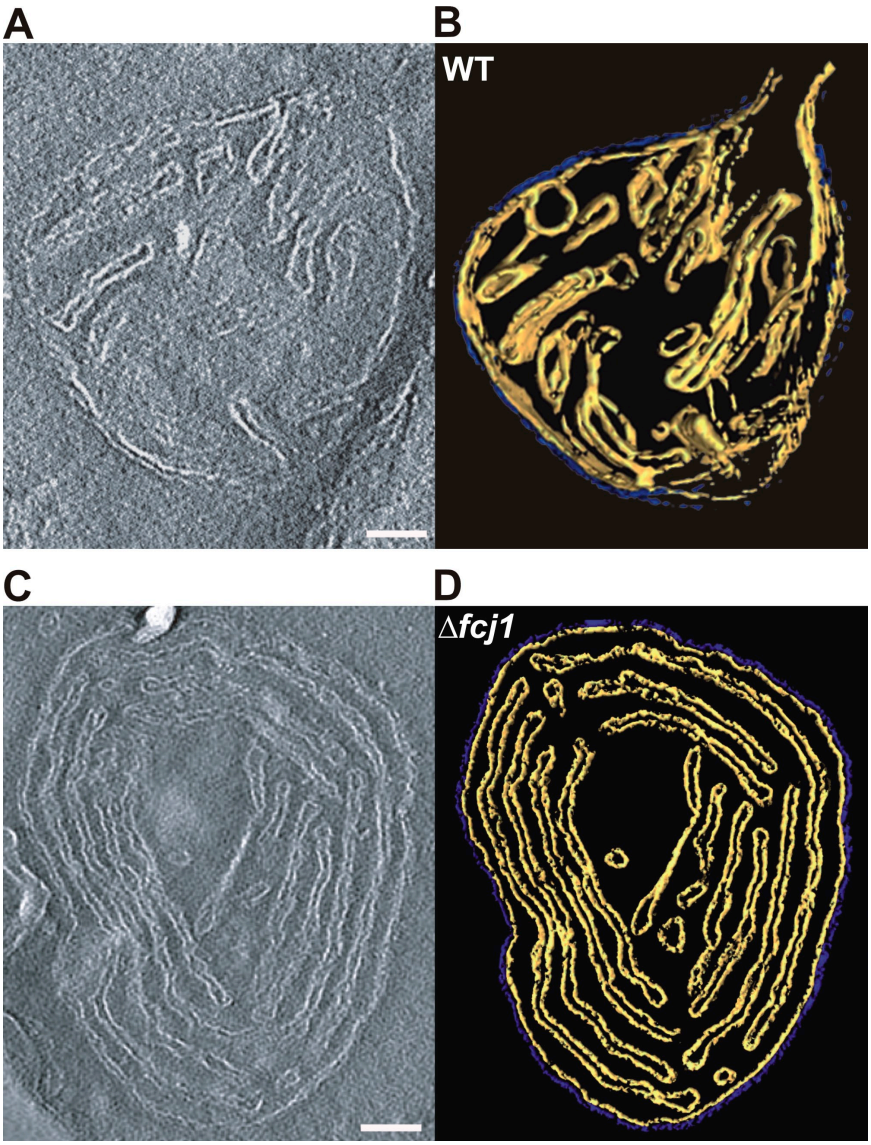


Figure 3. **Cristae morphology is altered, and CJs are absent in cells lacking Fcj1.** (A–D) EM tomograms of chemically fixed yeast cells. (A) Single slice of a tomogram of a mitochondrion in a wild-type cell. (B) Surface-rendered view of A. (C) Single slice of a tomogram of a mitochondrion from a *Δfcj1* cell. (D) Surface-rendered view of C. The OM (blue) and IM (yellow) are shown. WT, wild type. Bars, 100 nm.

parallel lines with a square-like or a hexagonal arrangement (Fig. 4, D–G). The dimensions and relative distances of these structures corresponded very well to those of the $F_1$ part of the $F_1F_O$–ATP synthase (~10 × 10 × 10 nm). These highly abundant structures have been assigned to dimers or oligomers of $F_1F_O$ in numerous other studies (Allen et al., 1989; Dudkina et al., 2005, 2006; Minauro-Sanmiguel et al., 2005; Buzhynskyy et al., 2007; Strauss et al., 2008).

To provide further evidence that the zipperlike structures represent oligomers of $F_1F_O$, we deleted Su *e* or Su *g* of $F_1F_O$. Loss of these subunits is known to impair dimerization/oligomerization of $F_1F_O$ (Arnold et al., 1998). Indeed, neither in *Δfcj1/Δsu g* (Fig. 5 A) nor in *Δfcj1/Δsu e* mitochondria (not depicted) were the putative F1 particles arranged in a zipperlike manner. Rather, they were distributed randomly over the IM, which is in contrast to what was observed with *Δfcj1* mitochondria

Table II. **Analysis of electron micrographs of cells with disturbed IM organization upon deletion of Fcj1, Su *e*, or Su *g***

| Strain | Number of mitochondrial sections | Number of CJs | Number of CJs per mitochondrial section | Percentage of CJs connected to one or more CJs | Number of cristae tips | Number of cristae tips per mitochondrial section |
|---|---|---|---|---|---|---|
| WT | 65 | 120 | 1.8 | 0 | 245 | 3.8 |
| *Δfcj1* | 75 | 0 | 0 | 0 | 731 | 9.7 |
| *Δsu e* | 58 | 170 | 2.9 | 84.1 | 12 | 0.2 |
| *Δsu g* | 64 | 163 | 2.5 | 81.0 | 10 | 0.2 |

WT, wild type. The numbers of CJs and cristae tips per mitochondrial section were determined from electron micrographs of chemically fixed whole cells of the indicated strains grown at 30°C on complete liquid media containing 2% (vol/vol) lactate.

Published June 15, 2009

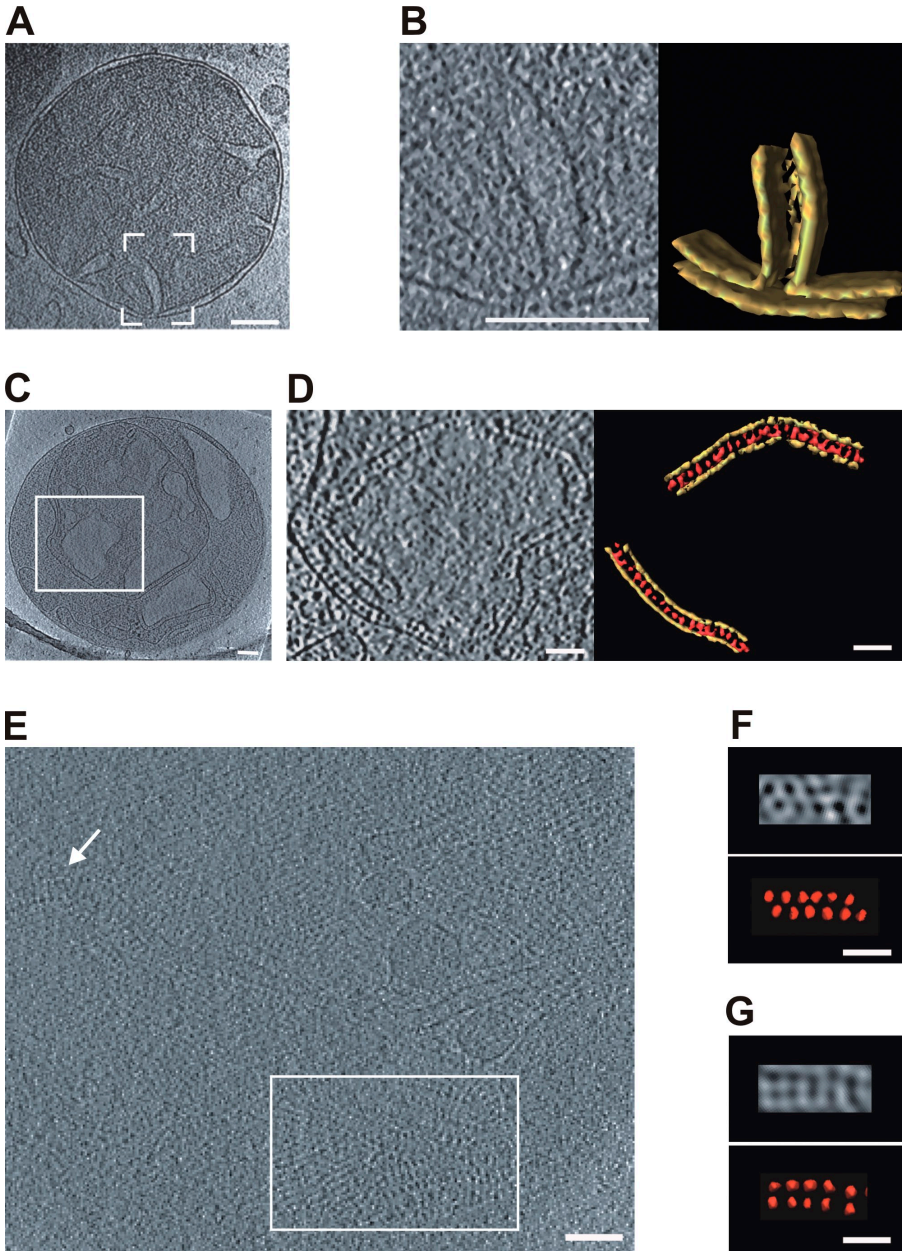


Figure 4. ***Δfcj1* mitochondria contain zipper-like structures typical of oligomers of the $F_1F_O$–ATP synthase.** Cryo-EM tomograms of isolated mitochondria. (A) Slice through a tomogram of a vitrified wild-type mitochondrion. (B) A CJ magnified (left) and surface rendered (right) corresponding to the boxed area in A is shown. Panels A and B are reprinted from Zick et al. (2009) with permission from *Biochimica et Biophysica Acta*. (C–G) *Δfcj1* mitochondria. (C) Slice through a tomogram of a vitrified *Δfcj1* mitochondrion. (D) Magnified view of boxed area in C (left) and surface-rendered representation (right) showing a zipperlike, regular arrangement with characteristics of the $F_1$ parts of $F_1F_O$–ATP synthase. The IM is shown in yellow, and $F_1F_O$–ATP synthases are shown in red. (E) A 10-nm thick slice of a tomogram cutting through particles typical of the $F_1$ parts of $F_1F_O$–ATP synthase in side views (arrow) and top views (boxed area). (F and G) Sections through the tomogram and volume-rendered top views of putative $F_1F_O$–ATP synthases arranged in double-row hexagonal stripes (F) and double-row square stripes (G) are shown. Bars: (A–C and E) 100 nm; (D, F, and G) 50 nm.

as a comparison (Fig. 5 B). This was confirmed by determining the distances between a large set of particles and their respective nearest neighbors. In *Δfcj1* mitochondria, the vast majority of observed distances was between 14 and 16 nm, whereas in *Δfcj1/Δsu g*, an apparently random distribution with a broad range of distances was detected (Fig. 5 C). Thus, the zipperlike structures in *Δfcj1* mitochondria indeed represent oligomers of $F_1F_O$ that can be disrupted by deletion of Su *e* or Su *g* of $F_1F_O$.

In intact wild-type mitochondria, $F_1F_O$ supercomplexes were neither observed in this study nor in other studies, probably as the result of the high protein density of the matrix and lack of contrast (Nicastro et al., 2000). The increased volume of mitochondria lacking Fcj1 (Table S1) probably caused a reduced protein density in the matrix and thereby facilitated the visualization of the supramolecular organization of $F_1F_O$ in intact mitochondria. Only in mitochondrial membrane fragments from wild-type yeast was an oligomeric arrangement of this complex previously observed (Buzhynskyy et al., 2007; Strauss et al., 2008). Collectively, the lack of Fcj1 correlates, on the one hand, with the absence of CJs and, on the other hand, with the appearance of regular arrangements of large protein complexes characteristic of $F_1F_O$ supercomplexes.

### Fcj1 has a direct role in determining the number and the architecture of CJs

To further study the role of Fcj1 in the formation of CJs, we used overexpression and down-regulation of Fcj1. Fcj1 was expressed from a plasmid in wild-type yeast cells under control of a doxycycline-repressible promoter. Wild-type cells containing the empty plasmid were also analyzed. Upon five- to 10-fold overexpression of Fcj1, the number of CJs per cell was increased two- to threefold as compared with control cells. The branching

Published June 15, 2009

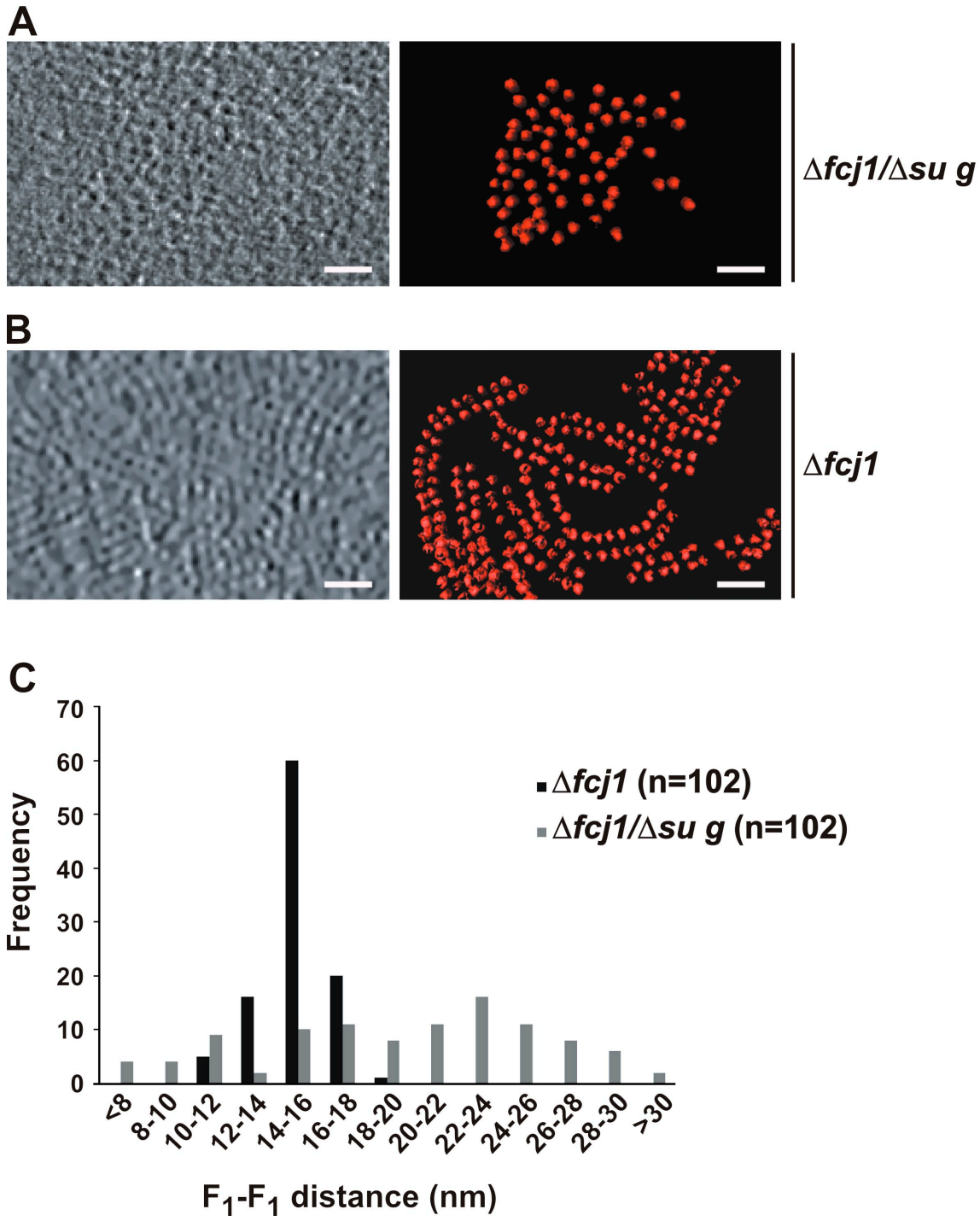


Figure 5. **Zipperlike structures observed in *Δfcj1* mitochondria depend on the presence of dimer-specific Su *e* and Su *g* of $F_1F_O$–ATP synthase.** Cryo-EM tomograms of isolated mitochondria of indicated strains. (A) Top views of putative $F_1F_O$–ATP synthases in *Δfcj1/Δsu g* mitochondria (left) and a surface-rendered representation (right) are shown. (B) Top views of putative $F_1F_O$–ATP synthases in *Δfcj1* mitochondria (left; magnified view of boxed area in Fig. 4 E) and a surface-rendered representation (right) are shown. (C) Frequency distribution of $F_1$–$F_1$ distances. The center to center distance of an $F_1$ particle to its nearest neighbor was determined for cryo-EM tomograms of isolated mitochondria of the indicated strains (*n* = 102 for both strains). Bars, 50 nm.

of cristae, which is very rarely observed in wild-type cells, was increased ∼17-fold in cells overexpressing Fcj1 (Fig. 6 A). Moreover, the diameter of CJs appeared enlarged and showed a higher variation when Fcj1 was overexpressed (Fig. 6, A and B). Thus, Fcj1 overexpression promotes the formation of additional CJs and alters the molecular architecture of CJs.

Down-regulation of Fcj1 led to a progressive decrease of the number of CJs as well as of cristae branches (Fig. 6, C and D). These alterations of cristae morphology occurred already at the early time points (13.5 and 23 h). Mitochondria with the characteristics of the *Δfcj1* phenotype with continuous concentric stacks of IM appeared at later time points (37.5 and 47.5 h).

Published June 15, 2009

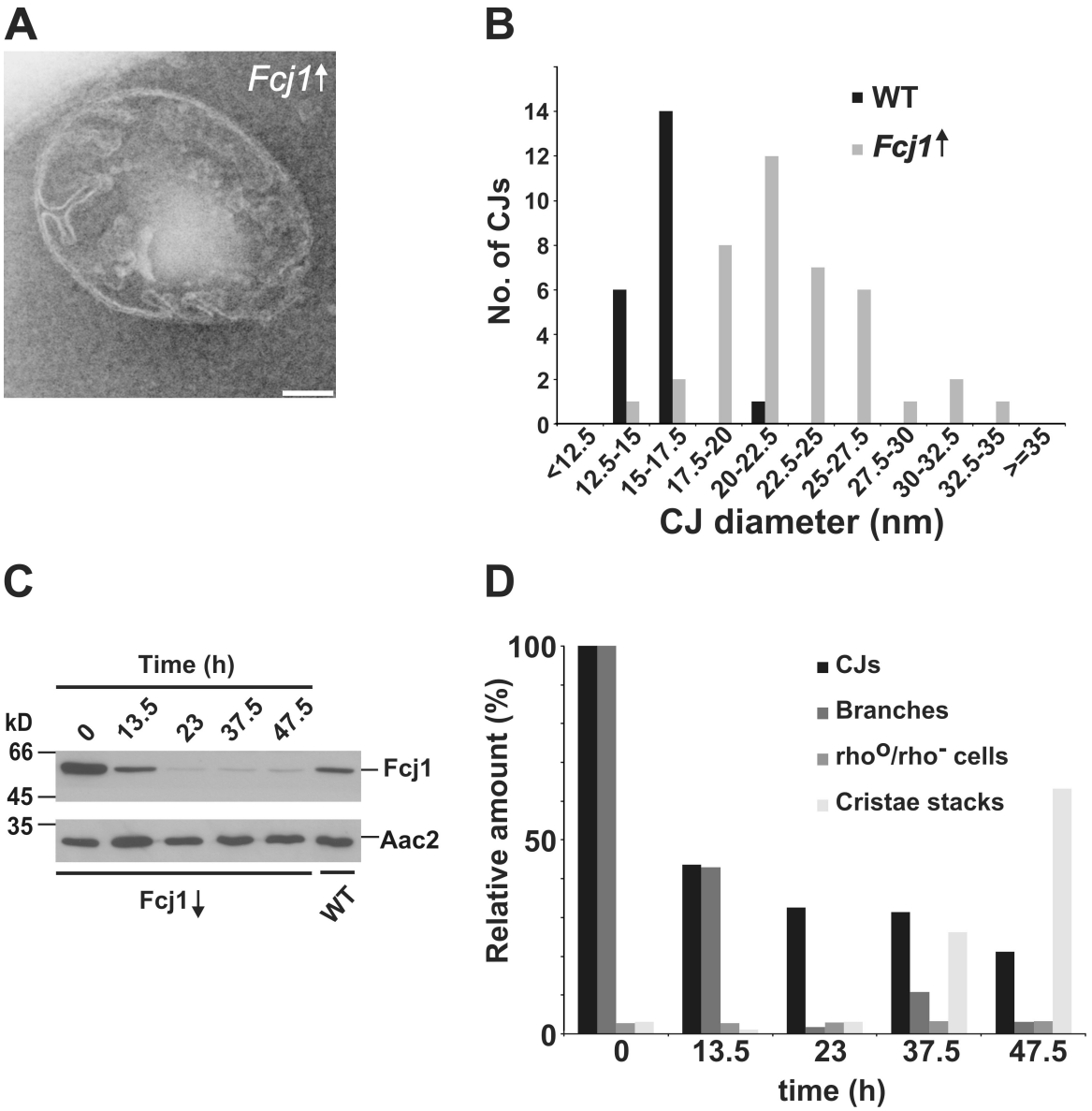


Figure 6. **Fcj1 is directly involved in determining the number and the architecture of CJs.** (A) Electron micrograph of a mitochondrion in a section of chemically fixed cells overexpressing Fcj1. (B) Distribution of diameters of CJs in wild-type (WT) control strain (W303) containing empty pCM189 plasmid ($n$ = 21) and Fcj1-overexpressing strain (W303) containing pCM189-Fcj1 plasmid (Fcj1↑; $n$ = 40). Cells were grown on nonfermentable, selective minimal media. A histogram of the number of diameters within the indicated ranges was plotted for both strains. (C and D) Fcj1 was down-regulated in a *Δfcj1* strain harboring the pCM189-Fcj1 at different times after doxycycline addition. Wild-type control as in B was used. (C) Expression levels of Fcj1 were monitored by Western blot analysis. (D) Phenotypic analysis of down-regulation of Fcj1. The number of CJs and branches per mitochondrial section ($m_{0\ h}$ = 26; $m_{13.5\ h}$ = 69; $m_{23\ h}$ = 49; $m_{37.5\ h}$ = 66; $m_{47.5\ h}$ = 57) was determined from electron micrographs of chemically fixed whole cells after the indicated time periods of down-regulation (m = number of mitochondrial sections). The number of CJs and cristae branches per mitochondrial section before down-regulation of Fcj1 (0 h) was defined as 100%. The number of $rho^0/rho^-$ cells and of cells containing cristae stacks is related to the number of total cells at each time point.

The incomplete disappearance of CJs is attributed to the incomplete down-regulation of Fcj1 (Fig. 6 C). The formation of $rho^0/rho^-$ cells was not observed in the course of the experiment, excluding the possibility that our observations are caused by a secondary loss of mtDNA. In summary, these observations strongly suggest a direct involvement of Fcj1 in CJ formation.

### Unchanged levels of Su *e* or Su *g* of the $F_1F_O$–ATP synthase in *Δfcj1* cells

Mutant strains lacking Su *e* or Su *g* of the $F_1F_O$–ATP synthase were reported to have altered cristae morphology (Paumard et al., 2002). Therefore, we asked whether protein levels of Su *e* or Su *g* were altered in *Δfcj1* cells and also whether levels of Fcj1 were altered in *Δsu e* or *Δsu g* cells. In the absence of Fcj1, similar levels of Su *e* or Su *g* were observed (Fig. 7 A). Thus, altered cristae morphology in *Δfcj1* mutant cells was not caused by a change in the levels of Su *e* or Su *g*. Likewise, Fcj1 levels were unaffected in *Δsu e* and *Δsu g* mutant cells, suggesting that Fcj1 is not responsible for the altered cristae morphology described for these mutants (Paumard et al., 2002). In addition, deletion of Fcj1 had no effect on the levels of several nuclear as well as mitochondrially encoded proteins that are involved in mitochondrial

Published June 15, 2009

functions such as mitochondrial protein import, mitochondrial fusion and fission machineries, and oxidative phosphorylation (Fig. 7 A). Notably, levels of proteins involved in determining mitochondrial morphology such as Mgm1, Fzo1, Fis1, and Dnm1 were not affected. Consistent with this, mitochondria in *Δfcj1* cells formed a tubular, albeit altered, network. The formation of the short isoform of Mgm1 (s-Mgm1) was also not impaired. This further supports our conclusion that mitochondrial energy production and protein import are functional in cells lacking Fcj1 as both processes are required for the formation of s-Mgm1 (Herlan et al., 2004).

### Fcj1 impairs oligomerization of the $F_1F_O$–ATP synthase

In view of the presence of a zipperlike arrangement of $F_1$ particles in *Δfcj1* mitochondria, we asked whether Fcj1 affects oligomerization of $F_1F_O$. First, we determined whether solubilization of $F_1F_O$ with a mild detergent depends on the level of Fcj1. Mitochondria isolated from wild-type cells, cells overexpressing Fcj1, and cells lacking Fcj1 were solubilized with digitonin. The proportion of nonsolubilized $F_1F_O$–ATP synthase subunits (F1β and Atp4) was highest in mitochondria lacking Fcj1, lower in wild type, and lowest in cells overexpressing Fcj1 (Fig. 7 B). The solubilization of other IM proteins such as Dld1 and Aac2 did not show such a dependence on the level of Fcj1. The nonsolubilized fraction of the $F_1F_O$–ATP synthase could subsequently be solubilized with Triton X-100. Apparently, $F_1F_O$ forms a high molecular mass complex that is less easily dissociated by digitonin in mitochondria lacking Fcj1.

We then examined the supramolecular organization of $F_1F_O$ by blue native PAGE (BN-PAGE) and in-gel visualization of its ATPase activity. Formation of monomers, dimers, and putative tetramers of $F_1F_O$ was observed in mitochondria of all strains (Fig. 7 C). Higher order oligomers were observed in *Δfcj1* mitochondria even at high digitonin concentrations, only at very low concentrations in wild-type mitochondria, and not when Fcj1 was overexpressed. These high molecular mass complexes of $F_1F_O$ represent a small subpopulation of the soluble fraction. They were very stable even at high digitonin to protein ratios when Fcj1 was lacking but not when Fcj1 was present. Overexpression of Fcj1 impaired the formation of these higher oligomers markedly and also decreased the amount of the tetrameric forms (Fig. 7 C and Fig. S5 A). The amount of dimers and monomers was not affected significantly. Likewise, the abundance of higher oligomers of $F_1F_O$ when determined by SEC was dependent on the presence of Fcj1 (Fig. 7 D). The majority of Fcj1 was recovered in the fractions corresponding to the higher oligomeric forms of $F_1F_O$ (>2 MD), showing that Fcj1 is present in a high molecular mass complex. Thus, the size of $F_1F_O$ oligomers was considerably larger upon solubilization with digitonin as compared with solubilization with Triton X-100 (Fig. S2). Collectively, various lines of evidence, including biochemical data as well as EM tomography, show that Fcj1 affects the stability of $F_1F_O$ oligomers in an adverse manner but obviously does not influence that of the dimers of this complex.

### Fcj1 acts in an antagonistic manner to Su *e* and Su *g* of the $F_1F_O$–ATP synthase

The observed effect of Fcj1 on the stability of oligomeric forms of $F_1F_O$ suggested a functional link between these proteins. Su *e* and Su *g* are known to be required for dimerization/oligomerization of $F_1F_O$ and are required for normal cristae morphology. To determine whether there exists a genetic interaction between these subunits and Fcj1, we determined the doubling times on a nonfermentable carbon source of each single and corresponding double deletion strain. The strain lacking Fcj1 was most severely impaired in growth on a nonfermentable carbon source, showing a ∼1.75-fold longer doubling time as compared with wild type (Fig. 8 A). Additional deletion of either Su *e* or Su *g* of $F_1F_O$ led to an efficient suppression of the growth defect of the *Δfcj1* strain. These double deletion strains had significantly shorter doubling times than the *Δfcj1* strain. This was further confirmed by drop dilution growth tests (Fig. 8 B). In conclusion, these data demonstrate a genetic interaction of Fcj1 with Su *e*/Su *g* of $F_1F_O$, placing all proteins in the same pathway. The latter subunits are promoting the assembly of $F_1F_O$–ATP synthase oligomers, whereas Fcj1 has the opposite effect. In the double deletion strains (*Δfcj1/Δsu e* and *Δfcj1/Δsu g*), the formation of $F_1F_O$–ATP synthase oligomers was not observed (Fig. S5 B). Dimers were present to a very low extent, resembling the phenotype of single deletions of Su *e* or Su *g*. This is consistent with the view that dimers are the building blocks for oligomerization of $F_1F_O$, as previously suggested (Paumard et al., 2002; Wittig et al., 2008). Collectively, Fcj1 interacts functionally with Su *e* and Su *g* in an antagonistic mode that appears crucial for the formation of CJs.

### Deletion of Su *e* and Su *g* leads to alterations of the IM structure of mitochondria

To relate the oligomeric states of $F_1F_O$ to the structure of cristae, we determined the number of cristae tips and the number of CJs in the deletion mutants of Su *e* and Su *g* and compared them with the numbers in wild-type and *Δfcj1* cells. Cristae tips per mitochondrial section were ∼2.5-fold more abundant in sections of *Δfcj1* cells than in wild type (Table II).

Mitochondria of strains lacking Su *e* or Su *g* were reported to contain onion-like structures and extended CMs (Paumard et al., 2002), but it was not investigated whether formation of CJs is affected. Therefore, we performed a quantitative analysis of CJs in these strains. Next to onion-like structures, we observed CJs in these strains, and the numbers of CJs per mitochondrial section were modestly increased compared with those in the corresponding wild type (Table II). Thus, Su *e* and Su *g* are not essential for CJ formation. However, CJs often appeared in pairs and were connected via CMs crossing a mitochondrial section, which is a structure rarely observed in wild type (Fig. 8, C and D; and Table II). In line with this observation, the number of cristae tips per mitochondrial section observed in *Δsu e* and *Δsu g* mitochondria was extremely low, ∼20 times lower than in wild type (Table II). Moreover, branching of cristae was found in 27% and 9% of mitochondrial sections of *Δsu e* and *Δsu g* strains, respectively, but not in sections of the corresponding wild-type strain (Fig. 8, C and D). Furthermore, the mean diameters of CJs in *Δsu e* and *Δsu g* cells were increased, although to a smaller extent

Published June 15, 2009

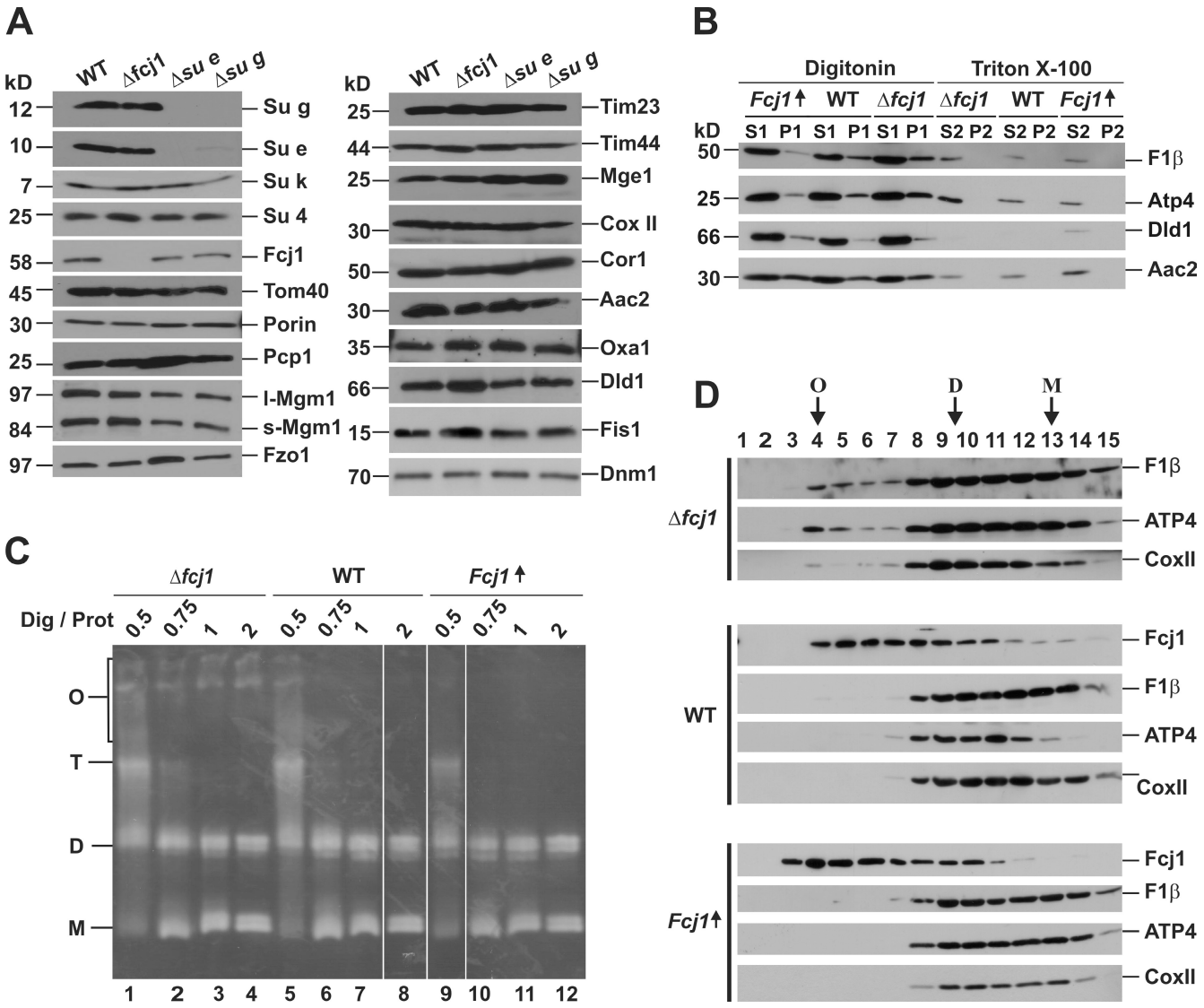


Figure 7. **Fcj1 reduces the stability of $F_1F_O$–ATP synthase oligomers.** (A) Protein levels in wild-type (WT), *Δfcj1*, *Δsu e*, and *Δsu g* mitochondria. Aliquots were subjected to SDS-PAGE and decorated with the indicated antibodies. (B) Solubility of $F_1F_O$–ATP synthase in detergents. Isolated mitochondria of Fcj1-overexpressing (Fcj1↑), wild-type, and *Δfcj1* strains were solubilized in digitonin and centrifuged to obtain supernatant (S1) and pellet (P1) fractions. Nonsolubilized material (P1) was treated with Triton X-100 and centrifuged to obtain supernatant (S2) and pellet (P2) fractions. Aliquots were analyzed by Western blotting with the indicated antibodies. (C) BN-PAGE analysis. Wild-type, *Δfcj1*, and Fcj1-overexpressing mitochondria (400 µg) were solubilized at the indicated ratios of digitonin/protein (Dig/Prot; wt/wt) and subjected to BN-PAGE and to analysis in-gel of $F_1F_O$–ATPase activity. All lanes were originated from a single gel at identical image settings, but lanes 8 and 9 were cut and pasted in the appropriate order for clarity. (D) SEC. Wild-type, *Δfcj1*, and Fcj1-overexpressing mitochondria were solubilized at a digitonin/protein ratio of 1 (wt/wt) and fractionated by Superose 6 gel filtration chromatography, and aliquots were analyzed by Western blotting. The oligomeric forms of the $F_1F_O$–ATP synthase (O, oligomers; T, tetramers; D, dimers; M, monomers) are indicated as size markers.

than in cells with overexpressed Fcj1, and showed a high variation (Fig. 8 E and not depicted). In wild-type cells, a slightly lower mean CJ diameter was measured when compared with the wild-type control shown in Fig. 6 B. We attribute this to different growth media (selective minimal vs. complete media) and strain backgrounds (W303 vs. BY4742; Table S2). We also investigated the ultrastructure of mitochondria of the double deletion strains *Δfcj1/Δsu e* and *Δfcj1/Δsu g*. These mitochondria were characterized by the presence of internal, concentric or vesicle-like CMs and the virtual absence of CJs (Fig. S5, C amd D). In conclusion, Su *e* and Su *g*, on the one hand, promote the formation of cristae tips, and Fcj1, on the other hand, is necessary for formation of CJs. These two types of mitochondrial membrane proteins modulate the oligomeric state of $F_1F_O$ in an antagonistic manner. This suggests that the architecture of the cristae with its elements of the cristae endings, connections with the IBM, and perhaps also the planar arrangement of cristae sheets are controlled by the local concentrations of these two types of antagonistic proteins.

## Discussion

This study addresses the question of how the complex structure of cristae in mitochondria is determined on a molecular basis. In this study, we report on proteins that, in conjunction with

Published June 15, 2009

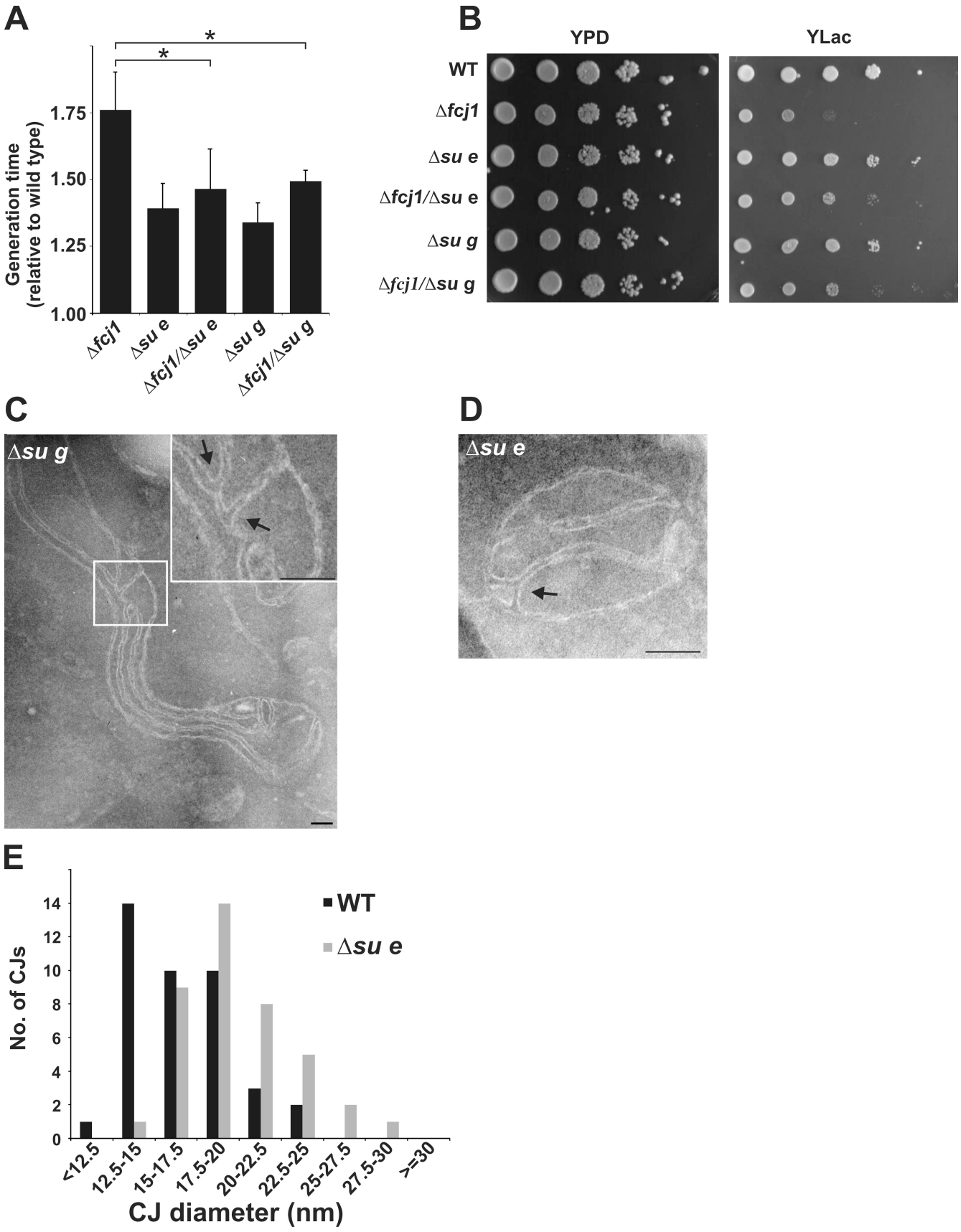


Figure 8. **Functional link between Fcj1 and the $F_1F_O$–ATP synthase.** (A and B) Genetic interaction of Fcj1 with Su *e* and Su *g*. (A) Generation times of the indicated strains (BY4742) grown in complete liquid lactate media during exponential growth at 30°C ($n = 4$). Error bars show standard deviations. Statistically significant differences (*, $P < 0.05$) according to a *t* test are indicated. (B) Growth of indicated strains tested by drop dilution in 1:10 steps on

Published June 15, 2009

$F_1F_O$–ATP synthase, determine cristae architecture. The IM protein Fcj1 plays an essential role in the formation of CJs and cristae shape. Su *e* and Su *g* of $F_1F_O$, whose depletion was previously shown to lead to onion-like cristae (Paumard et al., 2002), have an influence on cristae structure, which is opposing that of Fcj1. We present a model of how these components determine the structure of the various parts of cristae, which is based on our results as discussed in this study (Fig. 9, A and B).

Fcj1 is anchored to the IM by a single N-terminal transmembrane segment, exposing the major part of the protein to the intermembrane space. It undergoes homotypic interactions and is quite abundant with an estimated number of 5,730 molecules per cell (Ghaemmaghami et al., 2003). Yet, it is much less abundant than the major constituent of the IM, the $F_1F_O$–ATP synthase with an estimated number of 41,500 and 164,000 molecules for the F1α and F1β subunits, respectively (Ghaemmaghami et al., 2003). The mammalian protein mitofilin shares very low sequence similarity with Fcj1; however, it is likely to represent an orthologue on the basis of its depletion phenotype (John et al., 2005). Fcj1 is present at high levels at the base of CJs but is also present in other parts of cristae, although to a lesser extent. Deletion of Fcj1 leads to a loss of CJs. Overexpression results in an increase of the number of CJs and to internal branching of cristae, suggesting a direct role of Fcj1 in the formation of junctions. Fcj1 has a regulatory influence on the oligomeric state of $F_1F_O$. Deletion of Fcj1 leads to an increase in the level of $F_1F_O$ supercomplexes. This effect is also apparent upon morphological analysis of mitochondria lacking Fcj1. Cryo-EM revealed the formation of extensive $F_1F_O$ supercomplex structures in the matrix space between cristae of this strain. Consistent with these observations, overexpression of Fcj1 leads to a reduction of the level of $F_1F_O$ supercomplexes.

Manipulation of the levels of the $F_1F_O$ Su *e* and Su *g* yielded equally intriguing results. As previously documented, depletion of these subunits leads to accumulation of concentric cristae structures (Paumard et al., 2002). Deletion of either Su *e* or Su *g* has been reported to strongly favor the dissociation of the $F_1F_O$ into monomers (Arnold et al., 1998). Remarkably, this has no effect on the enzymatic activity of the ATP synthase. In this study, we show that these mitochondria contain CJs but exhibit a virtual absence of cristae tips. This goes along with a strongly increased number of bridgelike cristae that extend across whole sections of mitochondria, ending on both sides in CJs. Moreover, branching of cristae is observed in these mitochondria, much like in Fcj1-overexpressing cells. Thus, branching of cristae may represent internal CJs that emerge within a planar region of the cristae, a region in which CJs are normally absent.

In summary, our data show opposing functions of Fcj1 in relation to $F_1F_O$ Su *e* and Su *g*. Fcj1 is obviously critical for formation of CJs, whereas formation of cristae tips requires Su *e* and Su *g*. This is in line with the specific enrichment of these components within the respective regions of the IM, as revealed by quantitative immunogold labeling. It appears to be their relative distribution that determines cristae structure in mitochondria.

Building on our results, we propose a working hypothesis for the molecular basis of the generation of CJs and cristae tips. In the mitochondria of most species and organs, the following structural elements can be discriminated (Fig. 9, A and B). The cristae sheets are made up of two leaves of IM arranged in close apposition, leaving a narrow intermembrane space in between. These sheets are delimitated by tips or rims, in which the lipid bilayer is bending over, showing a strong positive curvature. At their base, the cristae are connected to the IBM, which forms a kind of second envelope tightly apposed to the OM. These connections, the CJs, have a rather complex 3D architecture. At the base where they open out into the IBM, the membrane exhibits negative curvature. It is followed by a narrow tubular neck region with highly positive curvature. This structure widens out into the planes of the cristae, a region in which both negative and positive curvatures are present.

According to our model, Fcj1 directly or indirectly interferes with the formation of higher oligomers and thereby favors negative membrane bending. By this mechanism, the presence of Fcj1 affects the building of the bases of CJs. However, in the regions where the formation of higher oligomeric forms of $F_1F_O$ is not disturbed, these oligomers impose a positive curvature on the membrane and thereby favor the formation of cristae tips. The idea of $F_1F_O$ oligomers introducing a positive curvature to the IM and leading to tip formation has also been put forward in a recent study (Strauss et al., 2008). Our findings attribute this effect to the action of Su *e* and Su *g*. As we show in this study, they are both enriched in the rim region, and their absence leads to a virtual absence of cristae tips. However, their lower abundance in CJs supports negative curvature. Interestingly, Fcj1 is present in very low amounts in cristae necks, the IM region connecting the base of CJ with the cristae sheets. This membrane has an extremely high positive curvature. Thus, we suggest that the ratios of Fcj1 to Su *e*/Su *g* are decisive in shaping cristae. The sheets of cristae appear to contain both Fcj1 and Su *e*/Su *g*, and this may determine their planar shape. A balanced distribution of these antagonistic components may also be necessary for the dynamics and fission/fusion of cristae. A dynamic nature of cristae was proposed previously (for reviews see Mannella et al., 2001; Mannella, 2006b) based on EM tomography studies of isolated mitochondria showing that cristae morphology apparently is reversibly changing under various physiological conditions (for reviews see Mannella et al., 2001; Mannella, 2006b; Zick et al., 2009).

Altogether, our hypothesis can explain all of the findings presented in this study and in other studies (Paumard et al., 2002; Strauss et al., 2008). It does not exclude that other components such as prohibitins or OPA1 or others yet to be identified also contribute to CJ and cristae tip formation (for reviews

fermentable (yeast peptone dextrose [YPD]) and respiratory (lactate medium [YLac]) carbon sources. (C and D) Electron micrographs of mitochondria of chemically fixed *Δsu g* (C) and *Δsu e* (D) cells. Branches are indicated by arrows. Enlargement of the indicated box is shown as an inset in C. (E) Diameters of CJs in electron micrographs of mitochondrial sections of wild-type (WT; m = 40) and *Δsu e* strains (m = 40; m = number of mitochondrial sections). Histograms of the number of observed diameters within the indicated ranges are shown. Bars, 100 nm.

Published June 15, 2009

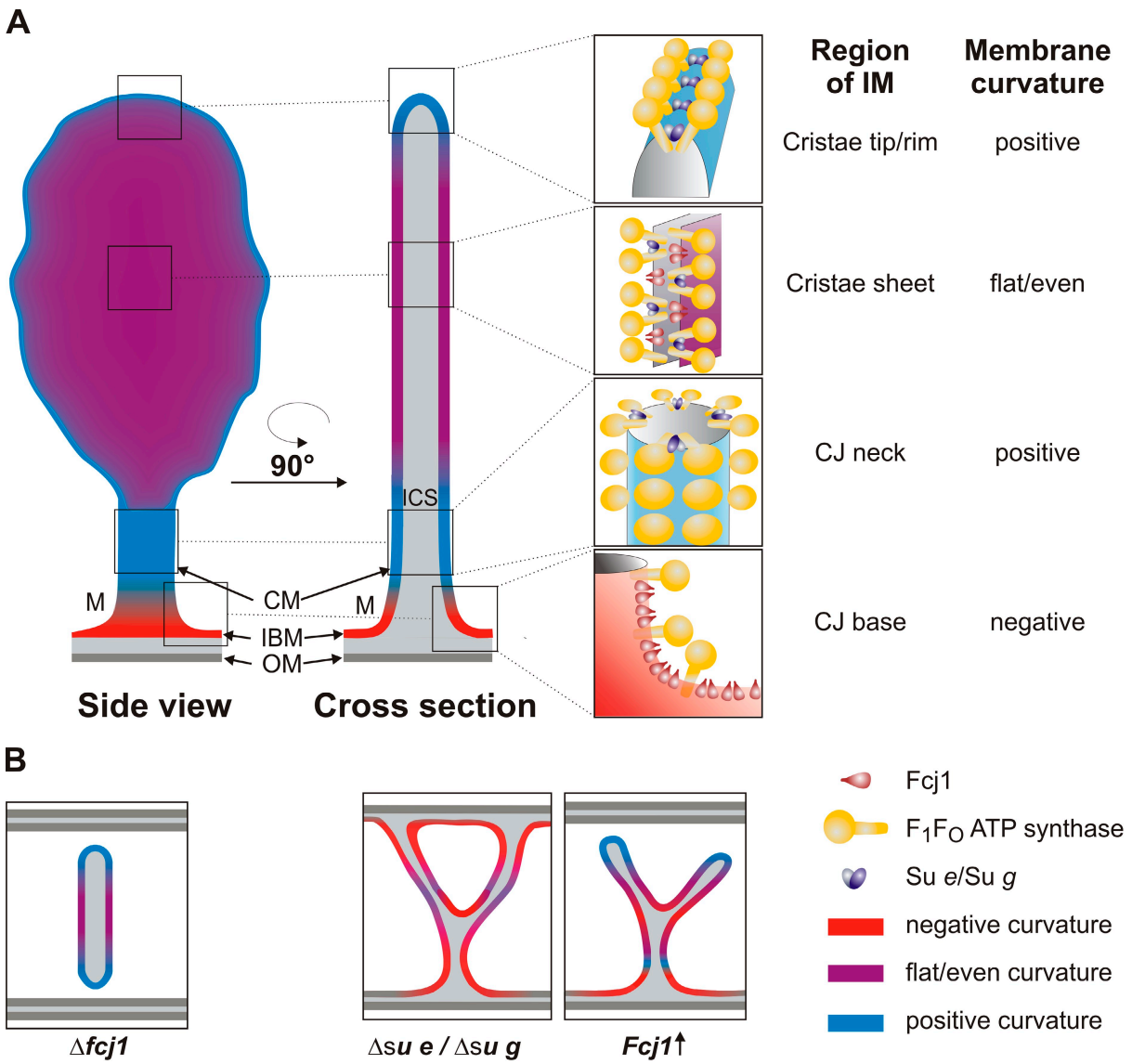


Figure 9. **Working model of the formation of cristae and CJs in mitochondria.** (A) Schematic representation of membrane curvatures at distinct regions of the CM and of the submitochondrial localization of Fcj1 and Su *e* and Su *g* in wild-type mitochondria. Positive membrane curvature is indicated in blue, negative curvature in red, and regions with both or no apparent curvature are colored in purple. An overview of a representative cristae sheet with one CJ is shown in side view (left) or as a cross section after 90° rotation (middle). Enlargements of boxed areas in 3D view show the proposed arrangement of Fcj1, Su *e*/Su *g*, and of $F_1F_O$ in the respective regions of the CM and their influence on membrane curvature. (B) Schematic representation of membrane curvature in CM structures observed in the indicated mutant mitochondria. Upon depletion of Fcj1, positive curvatures of the CM are predominating, whereas membrane structures that require negative bending of the membrane are absent. The lack of Su *e*/Su *g* leads to an apparent reduction in positive membrane curvatures, which results in an enlargement of CJ diameter, branching of cristae, and a strong reduction in the number of apparent cristae tips. Increased levels of Fcj1 produce a similar phenotype. However, the formation of cristae tips is not affected in this mutant. ICS, intracristal space; M, matrix space.

see Merkwirth and Langer, 2009; Zick et al., 2009). Also, it raises several intriguing questions such as how Fcj1 is recruited to the base of the CJ. Fcj1 itself or a possible reaction partner may interact with the OM and thereby anchor CJs to the OM. Of particular interest are the physical details of Fcj1 and Su *e*/Su *g* interaction with $F_1F_O$ and how these interactions regulate membrane curvature. Finally, an intriguing aspect is the obvious problem of how cristae stacks are formed when CJs are lacking and how protein import and complex assembly in the CM occurs in this situation. One possibility would be that there is a rapid fusion/fission mechanism of cristae to and from the IBM. The life time of these connections might be too short lived to be seen by EM but long enough for diffusion of newly inserted proteins and lipids. Several other explanations may seem equally possible. In any case, it will be a great challenge to find out how mitochondria can survive the virtual complete absence of CJs and still maintain mitochondrial function and inheritance.

## Materials and methods

### Strains and growth conditions

The strains and plasmids used are listed in Tables S2 and S3. Culturing of yeast strains was performed using standard methods (Sherman et al., 1986) at 30°C on complete liquid media containing 2% (vol/vol) lactate. Strains containing plasmids (Table S2) were grown on selective liquid

Published June 15, 2009

media containing 2% (vol/vol) lactate supplemented with 0.1% (wt/vol) glucose. For overexpression of Fcj1, the wild type and the *Δfcj1* strain containing the plasmid pCM189-Fcj1 were grown in the absence of doxycycline. For down-regulation of Fcj1, the same plasmid was used in a *Δfcj1* strain, and 20 µg/ml doxycycline was added to the medium. Drop dilution growth tests were performed with 1:10 dilution steps and incubation on yeast peptone dextrose and lactate medium plates for 2–4 d at 24°C. $Rho^0/rho^-$ cell formation was determined on complete glycerol plates supplemented with 0.1% (wt/vol) glucose.

**Fractionation of yeast cells**

Yeast total cell extracts were prepared by alkaline lysis as previously described (Herlan et al., 2003). Cellular subfractionation of yeast cells was performed as previously described (Rowley et al., 1994). To extract peripherally bound membrane proteins, 10 mg/ml of mitochondria was swollen by dilution to a final concentration of 1 mg/ml in 20 mM Hepes/KOH, pH 7.4. After the addition of an equal volume of freshly prepared 0.2 M Na carbonate solution or 2 M NaCl solution, samples were incubated for 30 min at 4°C and centrifuged at 92,000 *g* for 30 min at 4°C. Equal fractions of membrane-associated and soluble proteins were analyzed by SDS-PAGE and immunoblotting. Spheroplasting of yeast cells, preparation of mitochondria, generation of mitoplasts, and PK treatment were performed according to standard procedures (Sirrenberg et al., 1996).

**Recombinant DNA techniques**

The yeast strain *Δfcj1* (W303 background) was obtained by genomic integration of the PCR product synthesized from the plasmid pFA6aHIS3Mx6 (Wach et al., 1997) using the primers Fcj1-HIS3 upstream and Fcj1-HIS3 reverse. The deletion of Fcj1 was verified by PCR using the primers Fcj1 upstream and Fcj1 downstream. pCM189-Fcj1 was generated by amplifying *Fcj1* (YKR016w) by PCR from yeast genomic DNA using *Pyrococcus furiosus* polymerase (Agilent Technologies) and Fcj1 forward and overexpression Fcj1 reverse primers (Table S4) and cloning into the pCM189 yeast overexpression vector using BamHI–NotI restriction sites. For the generation of pYX242–Fcj1-$His_6$ or pYX242–Fcj1-$His_{12}$, the primers Fcj1 upstream and Fcj1-$His_6$ reverse or Fcj1 upstream and Fcj1-$His_{12}$ reverse, respectively, were used, and the PCR products were cloned into pYX242 using BamHI–XhoI restriction sites. Constructs or empty plasmids (Table S3) were transformed into the wild-type or the *Δfcj1* strain to allow growth of all strains in the same selective media.

**Antibody production**

Antisera against Fcj1 were raised in rabbits against a synthetic peptide corresponding to amino acid residues 214–226 of Fcj1 (CNTQYENSKREFEKN) coupled to activated ovalbumin (Pineda Antikörperservice).

**Protein purification**

Protein purification by TAP was adapted from a previous study (Puig et al., 2001). In brief, 25 µl of IgG Sepharose 6 Fast Flow (GE Healthcare) bead slurry was washed three times with TBS, once with 0.1 M Gly, pH 2.5, again three times with TBS, and once with solubilization buffer (10 mM Tris/HCl, pH 8.0, 150 mM NaCl, 1% [vol/vol] Triton X-100, and protease inhibitors [complete protease inhibitor cocktail; Roche]), 5 mM EDTA, 1 mM PMSF, 0.5 mM 1,10-phenanthroline, 2 µg/ml aprotinin, and 1 µg/ml pepstatin. 1 mg of isolated mitochondria (Fcj1-TAP, Fcj1-His, or Fcj1-TAP–Fcj1-His; Table S2) was solubilized for 30 min on ice in 100 µl of solubilization buffer. The samples were centrifuged for 20 min at 57,000 *g*, and the supernatants were loaded onto the prepared IgG Sepharose beads. After incubation for 1 h at 4°C, the beads were washed with solubilization buffer containing 0.1% (vol/vol) Triton X-100, and bound proteins were eluted with 2× Laemmli sample buffer for 3 min at 95°C and analyzed by SDS-PAGE and Western blotting.

Purification by nickel nitrilotriacetic acid binding of His-tagged proteins was performed as described previously (Mokranjac et al., 2005). In brief, 3 mg of mitochondria prepared from cells expressing tagged versions of Fcj1 (Fcj1-$His_{12}$, Fcj1-TAP–Fcj1-$His_6$, or Fcj1 full length as a control; Table S2) were solubilized in solubilization buffer for 30 min on ice containing 5 mM imidazol without EDTA. After a clarifying spin, the supernatants were incubated for 1 h at 4°C with 30 µl of washed nickel nitrilotriacetic acid bead slurry (EMD). The beads were washed with solubilization buffer containing 0.1% (vol/vol) Triton X-100 and 30 mM imidazol. Bound proteins were eluted with Laemmli sample buffer at 95°C or with 300 mM imidazol at 4°C depending on the subsequent treatment of the samples. Bound material was analyzed either by Coomassie staining or subjected to SEC.

**Analysis of bioenergetic parameters of mitochondria**

Wild-type and *Δfcj1* cells were grown on a nonfermentable carbon source (see Strains and growth conditions), and enzymatic activities of oxidative phosphorylation of isolated mitochondria were assayed essentially as described previously (Velours et al., 2001). Oxygen consumption rates were measured with an Oxygraph (Hansatech Instruments) and analyzed by Oxyg32 version 2.25 software (Hansatech Instruments). 500 µg of freshly isolated mitochondria was resuspended in 2 ml of respiration buffer (250 mM sucrose, 5 mM KPi, pH 7.4, 1 mM EDTA, 6 mM $MgCl_2$, and 20 mM Hepes/KOH, pH 7.4). After adding 4 mM NADH, state IV respiration was measured. Further addition of 200 µM ADP allowed determination of state III respiration. To uncouple respiration from ATP synthesis, 3 µM carbonyl cyanide m-chlorophenylhydrazone was added, leading to maximal respiration rate. ATPase activity was measured with or without the addition of oligomycin to a final concentration of 10 µg/ml, as previously described (Velours et al., 2001). The membrane potential ($\Delta\psi$) was evaluated by measurement of fluorescence quenching of rhodamine123 as previously described (Emaus et al., 1986).

**Analysis of oligomeric $F_1F_O$–ATP synthase complexes**

To determine the solubility of $F_1F_O$, isolated mitochondria were incubated on ice for 30 min in digitonin solution at a digitonin/protein (wt/wt) ratio of 1 (150 mM NaCl, 20 mM Tris/HCl, pH 8, 5 mM EDTA, 1 mM PMSF, complete protease inhibitor cocktail, 0.5 mM 1,10-phenanthroline, 100 µg/ml α-macroglobulin, 2 µg/ml aprotinin, and 1 µg/ml pepstatin). After centrifugation at 4°C for 10 min at 13,000 *g*, nonsolubilized material was resolubilized with 1% (vol/vol) Triton X-100.

**SEC**

Isolated mitochondria were solubilized for 30 min on ice at a digitonin/protein ratio of 1 (wt/wt) or at a Triton X-100/protein ratio of 0.5 in 30 mM Hepes/HCl, pH 7.4, and 150 mM potassium acetate including protease inhibitors as indicated in the previous section and centrifuged for 10 min at 13,000 *g* before the cleared lysate was loaded on a Superose 6 size exclusion column (GE Healthcare; Meier et al., 2005).

**BN–PAGE**

500 µg of mitochondria was incubated for 30 min at 4°C in 50 µl of digitonin buffer (30 mM Hepes/HCl, pH 7.4, 150 mM potassium acetate, 10% glycerol, 1 mM EDTA, 2 mM ε-amino caproic acid, and 1 mM PMSF) at the indicated ratios of digitonin/protein (wt/wt) and centrifuged at 4°C for 20 min at 57,000 *g*. Analysis of supernatants by BN-PAGE and in-gel ATPase activity was performed essentially as previously described (Schagger, 2001; Bornhövd et al., 2006).

**Fluorescence microscopy**

For the visualization of mitochondria, yeast strains were transformed with plasmid pVT100U–mitochondrial GFP–expressing mitochondrial matrix-targeted GFP (Westermann and Neupert, 2000) and grown on selective lactate medium lacking Leu. Confocal images were taken with a confocal microscope (LSM 510; Carl Zeiss, Inc.) equipped with a 63× objective and a differential interference contrast (DIC) setting. For imaging, living cells were embedded in 1% low melting point agarose and observed at RT. 512 × 512–pixel images at 1-µm focal increments were recorded, simultaneously imaging mitochondrially targeted GFP and DIC. Images were processed with an LSM image browser (Carl Zeiss, Inc.). For analysis of mitochondrial volume, means of at least 10 cells per yeast strain and five focal increments per cell were scored for the ratio of mitochondrial GFP within the cell (DIC picture).

**EM and electron tomography**

EM on chemically fixed, cryosectioned yeast cells using the Tokuyasu method (Tokuyasu, 1989) and quantitative immuno-EM were performed as previously described (Vogel et al., 2006). Cells were immunogold labeled using the indicated antibodies and goat anti–rabbit IgG conjugated to 10-nm gold particles (Dianova). The location of gold particles in mitochondria with clearly resolvable CMs connected by CJs to the IBM was plotted onto a single empirically determined model. To quantitatively determine the relative density of a protein along the IM, the number of gold particles within a 14-nm distance for all points on the IM was determined by moving in silico along the IM in the model from the bottom to the top of the model. CJ diameters were measured in electron micrographs of whole yeast cells prepared by the Tokuyasu method (Tokuyasu, 1989). For this, the distances from center to center of IMs of a CJ opening at the top were measured in various CJs for each yeast strain.

Published June 15, 2009

### Cryopreparation of isolated mitochondria

Cryopreparation was performed essentially as previously described (Dubochet et al., 1988). Freshly prepared mitochondria were resuspended in isotonic Hepes buffer (10 mM Hepes, pH 7.4, 1 mM EDTA, and 600 mM sorbitol) at a protein concentration of 10 mg/ml. 3–5 µl of this mitochondrial suspension was applied onto an EM grid (R2/2; Quantifoil; or custom made) and mounted in a plunger equipped with a custom-made humidifying device (Cyrklaff et al., 1990). After adding 3–5 µl of fiducial marker solution (3-nm protein A–gold [Sigma-Aldrich] in isotonic Hepes buffer), excess liquid was removed, and the grids were rapidly frozen in liquid ethane slush and stored in liquid nitrogen.

### Cryo-EM of vitreous sections

Sample vitrification, cryosectioning, and imaging were performed as described previously (Al-Amoudi et al., 2004). In brief, spheroplasted yeast cells mixed with fiducial markers in isotonic buffer were soaked in 20% dextran (~40 kD), sucked in 300-µm diameter copper tubes and high pressure frozen at >2,000 bars using EMPACT1 (Leica). Vitreous samples were cryosectioned in the microtome (Ultracut UCT; Leica) with nominal thickness of sections of 120 nm and a final thickness of ~200 nm as the result of specimen compression using either a 35° cryodiamond knife (Diatome) or a 45° glass knife with a clearance angle of 6°.

### Electron tomography

Cryohydrated samples were mounted in a 70° tilt cryospecimen holder (model 626; Gatan GmbH) and examined in a cryoelectron microscope (CM 300; Philips) equipped with a field emission gun, a postcolumn energy filter (GIF 2002; Gatan GmbH), and a slow-scan charge-coupled device camera (Gatan GmbH) with 2,048 × 2,048 pixels. Low electron-dose series (4,000–5,000 electrons/nm$^2$) of typically 60–70 images were recorded using the Digital Micrograph package (Gatan GmbH) in tilt ranges between ±60° and ±70°, with 2° tilt intervals, at nominal magnifications of 43,000 (0.82 nm/pixel) or 52,000 (0.68 nm/pixel), and with an objective lens defocus of 6–10 µm. Chemically preserved material was imaged under similar conditions, but the areas selected for recording of tomographic tilt series were preirradiated with electron doses of >10,000 electrons/nm$^2$. Images of tilt series were aligned using fiducial markers and merged in 3D reconstructions by weighted back-projection using the EM image processing package (Hegerl, 1996) as well as the translocase of the mitochondrial OM package (Nickell et al., 2005) for postprocessing the volumes. The final thickness of EM tomograms was between 300 and 500 nm. The AMIRA visualization package (Mercury Computer Systems) was used for surface rendering of membranes and molecules in mitochondria in the original reconstructions as well as for displaying the results in figures.

### Online supplemental material

Fig. S1 shows that *FCJ1* (*AIM28/FMP13/YKR016W*) has very low sequence similarity to mitofilin. Fig. S2 shows that oligomeric protein complexes containing Fcj1 are the result of Fcj1 self-interaction. Fig. S3 shows the specificity of Fcj1-directed antibodies and immuno-EM in *Δfcj1* cells. Fig. S4 shows that the deletion of Fcj1 leads to altered cristae morphology. Fig. S5 shows the analysis of double deletion strains *Δfcj1/Δsu e* and *Δfcj1/Δsu g* and of a strain overexpressing Fcj1. Videos 1 and 2 show EM tomograms of chemically fixed wild-type and *Δfcj1 S. cerevisiae* cells, respectively. Video 3 shows a cryo-EM tomogram of isolated wild type *S. cerevisiae* mitochondrion. Videos 4 and 5 show cryo-EM tomograms of isolated *Δfcj1 S. cerevisiae* mitochondrion. Table S1 shows the quantitative analysis of wild-type and *Δfcj1* cells. Tables S2–S4 show the strains, plasmids, and oligonucleotides, respectively, used in this study. Online supplemental material is available at http://www.jcb.org/cgi/content/full/jcb.200811099/DC1.

We thank Drs. Carsten Bornhövd, Stéphane Duvezin-Caubet, Kai Hell, and Julio Ortiz for helpful discussions and Gabriele Ludwig and Margit Vogel for excellent technical assistance.

This work was supported by the Deutsche Forschungsgemeinschaft Sonderforschungsbereich 594 project B8 (grant to A.S. Reichert), the Cluster of Excellence Macromolecular Complexes at the Goethe University Frankfurt Deutsche Forschungsgemeinschaft Project EXC 115 (grant to A.S. Reichert), the Center for Integrated Protein Science München, the Fondation pour la Recherche Médicale (grant to V. Soubannier), and a Federation of European Biochemical Societies postdoctoral fellowship (to V. Soubannier). The first two authors contributed equally and are listed in alphabetical order.

Submitted: 19 November 2008
Accepted: 18 May 2009

## References

Al-Amoudi, A., J.J. Chang, A. Leforestier, A. McDowall, L.M. Salamin, L.P. Norlen, K. Richter, N.S. Blanc, D. Studer, and J. Dubochet. 2004. Cryo-electron microscopy of vitreous sections. *EMBO J.* 23:3583–3588.

Allen, R.D., C.C. Schroeder, and A.K. Fok. 1989. An investigation of mitochondrial inner membranes by rapid-freeze deep-etch techniques. *J. Cell Biol.* 108:2233–2240.

Arnold, I., K. Pfeiffer, W. Neupert, R.A. Stuart, and H. Schagger. 1998. Yeast mitochondrial F1F0-ATP synthase exists as a dimer: identification of three dimer-specific subunits. *EMBO J.* 17:7170–7178.

Bornhövd, C., F. Vogel, W. Neupert, and A.S. Reichert. 2006. Mitochondrial membrane potential is dependent on the oligomeric state of F1F0-ATP synthase supracomplexes. *J. Biol. Chem.* 281:13990–13998.

Buzhynskyy, N., P. Sens, V. Prima, J.N. Sturgis, and S. Scheuring. 2007. Rows of ATP synthase dimers in native mitochondrial inner membranes. *Biophys. J.* 93:2870–2876.

Cipolat, S., T. Rudka, D. Hartmann, V. Costa, L. Serneels, K. Craessaerts, K. Metzger, C. Frezza, W. Annaert, L. D'Adamio, et al. 2006. Mitochondrial rhomboid PARL regulates cytochrome c release during apoptosis via OPA1-dependent cristae remodeling. *Cell*. 126:163–175.

Claros, M.G., and P. Vincens. 1996. Computational method to predict mitochondrially imported proteins and their targeting sequences. *Eur. J. Biochem.* 241:779–786.

Cyrklaff, M., M. Adrian, and J. Dubochet. 1990. Evaporation during preparation of unsupported thin vitrified aqueous layers for cryo-electron microscopy. *J. Electron Microsc. Tech.* 16:351–355.

Daems, W.T., and E. Wisse. 1966. Shape and attachment of the cristae mitochondriales in mouse hepatic cell mitochondria. *J. Ultrastruct. Res.* 16:123–140.

DiMauro, S., E. Bonilla, M. Zeviani, M. Nakagawa, and D.C. DeVivo. 1985. Mitochondrial myopathies. *Ann. Neurol.* 17:521–538.

Dubochet, J., M. Adrian, J.J. Chang, J.C. Homo, J. Lepault, A.W. McDowall, and P. Schultz. 1988. Cryo-electron microscopy of vitrified specimens. *Q. Rev. Biophys.* 21:129–228.

Dudkina, N.V., J. Heinemeyer, W. Keegstra, E.J. Boekema, and H.P. Braun. 2005. Structure of dimeric ATP synthase from mitochondria: an angular association of monomers induces the strong curvature of the inner membrane. *FEBS Lett.* 579:5769–5772.

Dudkina, N.V., S. Sunderhaus, H.P. Braun, and E.J. Boekema. 2006. Characterization of dimeric ATP synthase and cristae membrane ultrastructure from *Saccharomyces* and *Polytomella* mitochondria. *FEBS Lett.* 580:3427–3432.

Emaus, R.K., R. Grunwald, and J.J. Lemasters. 1986. Rhodamine 123 as a probe of transmembrane potential in isolated rat-liver mitochondria: spectral and metabolic properties. *Biochim. Biophys. Acta*. 850:436–448.

Fawcett, D.W. 1981. The Cell. Second edition. W.B. Saunders, Philadelphia. 410–486.

Frey, T.G., and C.A. Mannella. 2000. The internal structure of mitochondria. *Trends Biochem. Sci.* 25:319–324.

Frey, T.G., C.W. Renken, and G.A. Perkins. 2002. Insight into mitochondrial structure and function from electron tomography. *Biochim. Biophys. Acta*. 1555:196–203.

Frezza, C., S. Cipolat, O. Martins de Brito, M. Micaroni, G.V. Beznoussenko, T. Rudka, D. Bartoli, R.S. Polishuck, N.N. Danial, B. De Strooper, and L. Scorrano. 2006. OPA1 controls apoptotic cristae remodeling independently from mitochondrial fusion. *Cell*. 126:177–189.

Ghaemmaghami, S., W.K. Huh, K. Bower, R.W. Howson, A. Belle, N. Dephoure, E.K. O'Shea, and J.S. Weissman. 2003. Global analysis of protein expression in yeast. *Nature*. 425:737–741.

Gilkerson, R.W., J.M. Selker, and R.A. Capaldi. 2003. The cristal membrane of mitochondria is the principal site of oxidative phosphorylation. *FEBS Lett.* 546:355–358.

Hegerl, R. 1996. The EM program package: a platform for image processing in biological electron microscopy. *J. Struct. Biol.* 116:30–34.

Herlan, M., F. Vogel, C. Bornhövd, W. Neupert, and A.S. Reichert. 2003. Processing of Mgm1 by the rhomboid-type protease Pcp1 is required for maintenance of mitochondrial morphology and of mitochondrial DNA. *J. Biol. Chem.* 278:27781–27788.

Herlan, M., C. Bornhövd, K. Hell, W. Neupert, and A.S. Reichert. 2004. Alternative topogenesis of Mgm1 and mitochondrial morphology depend on ATP and a functional import motor. *J. Cell Biol.* 165:167–173.

Icho, T., T. Ikeda, Y. Matsumoto, F. Hanaoka, K. Kaji, and N. Tsuchida. 1994. A novel human gene that is preferentially transcribed in heart muscle. *Gene*. 144:301–306.

John, G.B., Y. Shang, L. Li, C. Renken, C.A. Mannella, J.M. Selker, L. Rangell, M.J. Bennett, and J. Zha. 2005. The mitochondrial inner membrane protein mitofilin controls cristae morphology. *Mol. Biol. Cell*. 16:1543–1554.

Mannella, C.A. 2006a. The relevance of mitochondrial membrane topology to mitochondrial function. *Biochim. Biophys. Acta*. 1762:140–147.

Mannella, C.A. 2006b. Structure and dynamics of the mitochondrial inner membrane cristae. *Biochim. Biophys. Acta*. 1763:542–548.

Mannella, C.A., M. Marko, P. Penczek, D. Barnard, and J. Frank. 1994. The internal compartmentation of rat-liver mitochondria: tomographic study using the high-voltage transmission electron microscope. *Microsc. Res. Tech.* 27:278–283.

Mannella, C.A., D.R. Pfeiffer, P.C. Bradshaw, I.I. Moraru, B. Slepchenko, L.M. Loew, C.E. Hsieh, K. Buttle, and M. Marko. 2001. Topology of the mitochondrial inner membrane: dynamics and bioenergetic implications. *IUBMB Life*. 52:93–100.

Meeusen, S., R. DeVay, J. Block, A. Cassidy-Stone, S. Wayson, J.M. McCaffery, and J. Nunnari. 2006. Mitochondrial inner-membrane fusion and crista maintenance requires the dynamin-related GTPase Mgm1. *Cell*. 127:383–395.

Meier, S., W. Neupert, and J.M. Herrmann. 2005. Conserved N-terminal negative charges in the Tim17 subunit of the TIM23 translocase play a critical role in the import of preproteins into mitochondria. *J. Biol. Chem.* 280:7777–7785.

Merkwirth, C., and T. Langer. 2009. Prohibitin function within mitochondria: essential roles for cell proliferation and cristae morphogenesis. *Biochim. Biophys. Acta*. 1793:27–32.

Merkwirth, C., S. Dargazanli, T. Tatsuta, S. Geimer, B. Lower, F.T. Wunderlich, J.C. von Kleist-Retzow, A. Waisman, B. Westermann, and T. Langer. 2008. Prohibitins control cell proliferation and apoptosis by regulating OPA1-dependent cristae morphogenesis in mitochondria. *Genes Dev.* 22:476–488.

Minauro-Sanmiguel, F., S. Wilkens, and J.J. Garcia. 2005. Structure of dimeric mitochondrial ATP synthase: novel F0 bridging features and the structural basis of mitochondrial cristae biogenesis. *Proc. Natl. Acad. Sci. USA*. 102:12356–12358.

Mokranjac, D., D. Popov-Celeketic, K. Hell, and W. Neupert. 2005. Role of Tim21 in mitochondrial translocation contact sites. *J. Biol. Chem.* 280:23437–23440.

Munn, E.A. 1974. The Structure of Mitochondria. Academic Press, London. 465 pp.

Nicastro, D., A.S. Frangakis, D. Typke, and W. Baumeister. 2000. Cryo-electron tomography of neurospora mitochondria. *J. Struct. Biol.* 129:48–56.

Nickell, S., F. Forster, A. Linaroudis, W.D. Net, F. Beck, R. Hegerl, W. Baumeister, and J.M. Plitzko. 2005. TOM software toolbox: acquisition and analysis for electron tomography. *J. Struct. Biol.* 149:227–234.

Odgren, P.R., G. Toukatly, P.L. Bangs, R. Gilmore, and E.G. Fey. 1996. Molecular characterization of mitofilin (HMP), a mitochondria-associated protein with predicted coiled coil and intermembrane space targeting domains. *J. Cell Sci.* 109:2253–2264.

Olichon, A., E. Guillou, C. Delettre, T. Landes, L. Arnaune-Pelloquin, L.J. Emorine, V. Mils, M. Daloyau, C. Hamel, P. Amati-Bonneau, et al. 2006. Mitochondrial dynamics and disease, OPA1. *Biochim. Biophys. Acta*. 1763:500–509.

Paumard, P., J. Vaillier, B. Coulary, J. Schaeffer, V. Soubannier, D.M. Mueller, D. Brethes, J.P. di Rago, and J. Velours. 2002. The ATP synthase is involved in generating mitochondrial cristae morphology. *EMBO J.* 21:221–230.

Perkins, G., C. Renken, M.E. Martone, S.J. Young, M. Ellisman, and T. Frey. 1997. Electron tomography of neuronal mitochondria: three-dimensional structure and organization of cristae and membrane contacts. *J. Struct. Biol.* 119:260–272.

Perkins, G.A., J.Y. Song, L. Tarsa, T.J. Deerinck, M.H. Ellisman, and T.G. Frey. 1998. Electron tomography of mitochondria from brown adipocytes reveals crista junctions. *J. Bioenerg. Biomembr.* 30:431–442.

Perkins, G.A., M.H. Ellisman, and D.A. Fox. 2003. Three-dimensional analysis of mouse rod and cone mitochondrial cristae architecture: bioenergetic and functional implications. *Mol. Vis.* 9:60–73.

Pon, L., T. Moll, D. Vestweber, B. Marshallsay, and G. Schatz. 1989. Protein import into mitochondria: ATP-dependent protein translocation activity in a submitochondrial fraction enriched in membrane contact sites and specific proteins. *J. Cell Biol.* 109:2603–2616.

Puig, O., F. Caspary, G. Rigaut, B. Rutz, E. Bouveret, E. Bragado-Nilsson, M. Wilm, and B. Seraphin. 2001. The tandem affinity purification (TAP) method: a general procedure of protein complex purification. *Methods*. 24:218–229.

Renken, C., G. Siragusa, G. Perkins, L. Washington, J. Nulton, P. Salamon, and T.G. Frey. 2002. A thermodynamic model describing the nature of the crista junction: a structural motif in the mitochondrion. *J. Struct. Biol.* 138:137–144.

Rowley, N., C. Prip-Buus, B. Westermann, C. Brown, E. Schwarz, B. Barrell, and W. Neupert. 1994. Mdj1p, a novel chaperone of the DnaJ family, is involved in mitochondrial biogenesis and protein folding. *Cell*. 77:249–259.

Schagger, H. 2001. Blue-native gels to isolate protein complexes from mitochondria. *Methods Cell Biol.* 65:231–244.

Scorrano, L., M. Ashiya, K. Buttle, S. Weiler, S.A. Oakes, C.A. Mannella, and S.J. Korsmeyer. 2002. A distinct pathway remodels mitochondrial cristae and mobilizes cytochrome c during apoptosis. *Dev. Cell*. 2:55–67.

Sherman, F., G.R. Fink, and J.B. Hicks. 1986. Laboratory Course Manual for Methods in Yeast Genetics. Cold Spring Harbor Laboratory Press, Cold Spring Harbor, NY.

Sirrenberg, C., M.F. Bauer, B. Guiard, W. Neupert, and M. Brunner. 1996. Import of carrier proteins into the mitochondrial inner membrane mediated by Tim22. *Nature*. 384:582–585.

Strauss, M., G. Hofhaus, R.R. Schroder, and W. Kuhlbrandt. 2008. Dimer ribbons of ATP synthase shape the inner mitochondrial membrane. *EMBO J.* 27:1154–1160.

Taylor, S.W., E. Fahy, B. Zhang, G.M. Glenn, D.E. Warnock, S. Wiley, A.N. Murphy, S.P. Gaucher, R.A. Capaldi, B.W. Gibson, and S.S. Ghosh. 2003. Characterization of the human heart mitochondrial proteome. *Nat. Biotechnol.* 21:281–286.

Tokuyasu, K.T. 1989. Use of poly(vinylpyrrolidone) and poly(vinyl alcohol) for cryoultramicrotomy. *Histochem. J.* 21:163–171.

Velours, J., J. Vaillier, P. Paumard, V. Soubannier, J. Lai-Zhang, and D.M. Mueller. 2001. Bovine coupling factor 6, with just 14.5% shared identity, replaces subunit h in the yeast ATP synthase. *J. Biol. Chem.* 276:8602–8607.

Vogel, F., C. Bornhövd, W. Neupert, and A.S. Reichert. 2006. Dynamic subcompartmentalization of the mitochondrial inner membrane. *J. Cell Biol.* 175:237–247.

Wach, A., A. Brachat, C. Alberti-Segui, C. Rebischung, and P. Philippsen. 1997. Heterologous HIS3 marker and GFP reporter modules for PCR-targeting in *Saccharomyces cerevisiae*. *Yeast*. 13:1065–1075.

Wallace, D.C. 2005. A mitochondrial paradigm of metabolic and degenerative diseases, aging, and cancer: a dawn for evolutionary medicine. *Annu. Rev. Genet.* 39:359–407.

Werner, S., and W. Neupert. 1972. Functional and biogenetical heterogeneity of the inner membrane of rat-liver mitochondria. *Eur. J. Biochem.* 25:379–396.

Westermann, B., and W. Neupert. 2000. Mitochondria-targeted green fluorescent proteins: convenient tools for the study of organelle biogenesis in *Saccharomyces cerevisiae*. *Yeast*. 16:1421–1427.

Wittig, I., J. Velours, R. Stuart, and H. Schägger. 2008. Characterization of domain interfaces in monomeric and dimeric ATP synthase. *Mol. Cell. Proteomics*. 7:995–1004.

Wong, E.D., J.A. Wagner, S.V. Scott, V. Okreglak, T.J. Holewinske, A. Cassidy-Stone, and J. Nunnari. 2003. The intramitochondrial dynamin-related GTPase, Mgm1p, is a component of a protein complex that mediates mitochondrial fusion. *J. Cell Biol.* 160:303–311.

Wurm, C.A., and S. Jakobs. 2006. Differential protein distributions define two sub-compartments of the mitochondrial inner membrane in yeast. *FEBS Lett.* 580:5628–5634.

Zick, M., R. Rabl, and A.S. Reichert. 2009. Cristae formation-linking ultrastructure and function of mitochondria. *Biochim. Biophys. Acta*. 1793:5–19.

Published June 15, 2009

# Supplemental Material

JCB

Rabl et al., http://www.jcb.org/cgi/content/full/jcb.200811099/DC1

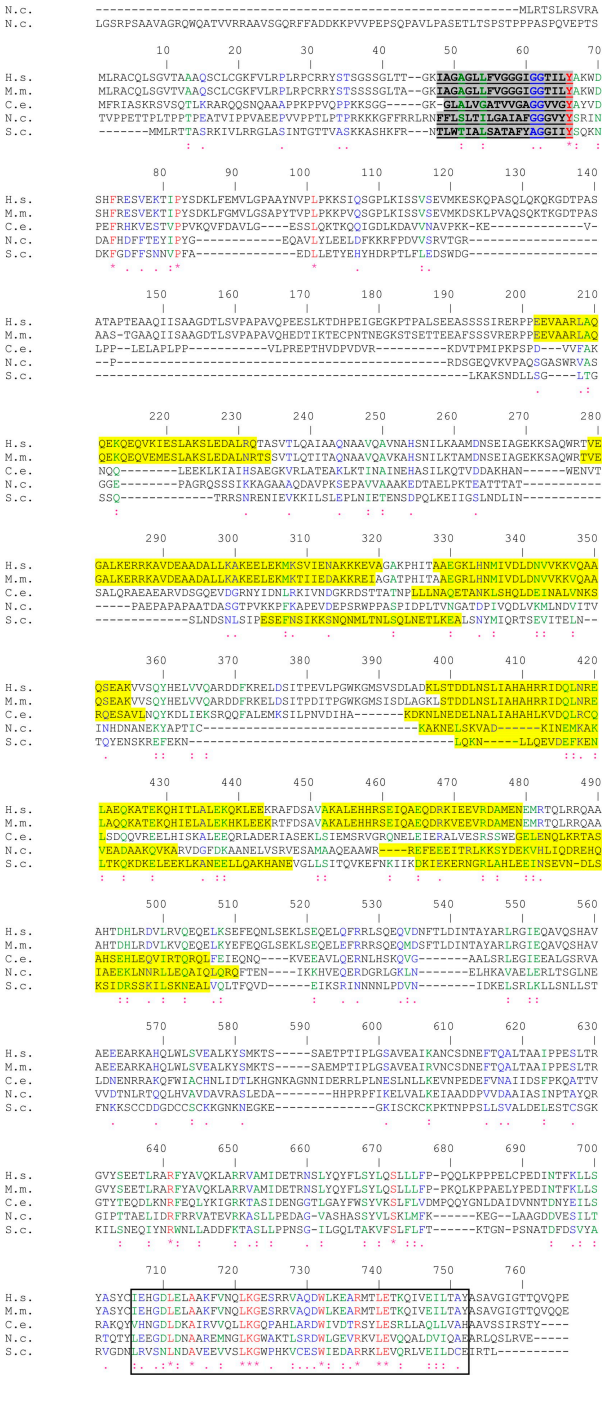

Figure S1. ***FCJ1* (*AIM28/FMP13/YKR016W*) has very low sequence similarity to mitofilin.** Amino acid sequences of mitofilin-related proteins Fcj1 (*S. cerevisiae* [S.c.]), Q7SFD8 (*Neurospora crassa* [N.c.]), Q22505 (*Caenorhabditis elegans* [C.e.]), mouse *IMMT* (Q8CAQ8; *Mus musculus* [M.m.]), and human *IMMT* (Q16891; *Homo sapiens* [H.s.]) were aligned using CLUSTALW (Thompson, J.D., D.G. Higgins, and T.J. Gibson. 1994. *Nucleic Acids Res.* 22:4673–4680) at the Pôle BioInformatique Lyonnais server (http://npsa-pbil.ibcp.fr). Amino acid residues are indicated as identical (asterisk; red), very similar (colon; green), and weakly similar (period; blue). Gaps are indicated by dashes. A conserved C-terminal domain is indicated by a box. The position of the single predicted transmembrane segment present in all species is underlined and highlighted in gray. Putative coiled-coil domains are highlighted in yellow.

Published June 15, 2009

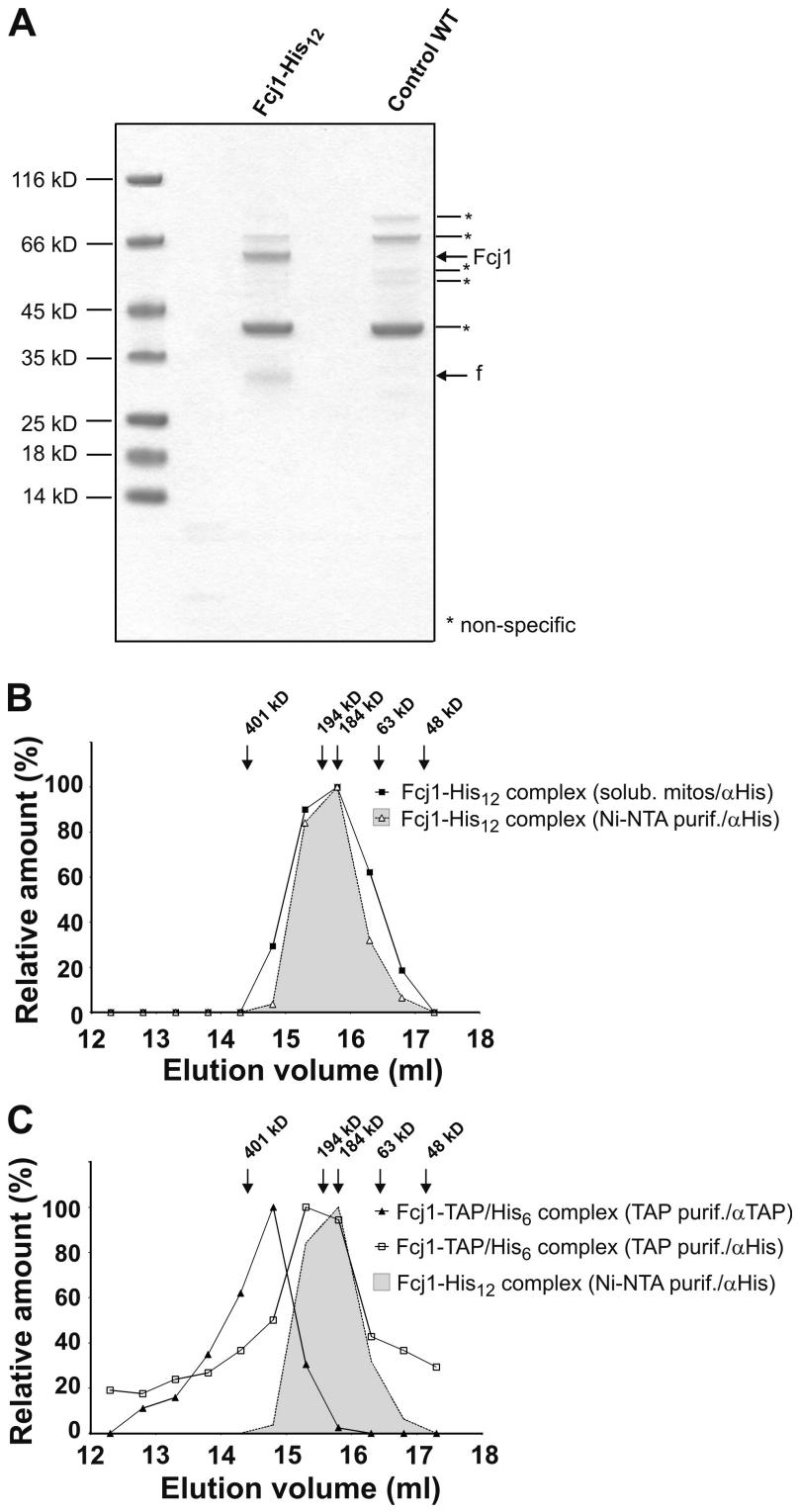


Figure S2. **Oligomeric protein complexes containing Fcj1 are caused by Fcj1 self-interaction.** (A) Nickel nitrilotriacetic acid pull-down of Fcj1 from solubilized mitochondria. A His-tagged variant of Fcj1 (Fcj1-$His_{12}$) and wild-type (WT) control were subjected to nickel nitrilotriacetic acid affinity purification. Bound material was analyzed by SDS-PAGE and Coomassie staining. Protein bands corresponding to Fcj1 and a degradation fragment of Fcj1 (f) were identified by immunoblotting (not depicted). Nonspecific protein bands are indicated by an asterisk. (B and C) Homo-oligomeric nature of the Fcj1 complex. (B) Mitochondria from cells expressing Fcj1-$His_{12}$ were isolated and either directly subjected to SEC on a Superose 6 column (closed squares) or nickel nitrilotriacetic acid (Ni-NTA) pull-down was performed, and the bound material was subjected to SEC (open triangles; gray). (C) Mitochondria from cells expressing both Fcj1 and Fcj1-TAP were solubilized and subjected to TAP affinity purification. Bound material was subjected to SEC. Analysis of SEC fractions was performed by SDS-PAGE and Western blotting with the indicated antibodies both against the His-tagged (open squares) and the TAP-tagged (closed triangles) versions of Fcj1. Bands were quantified by densitometry, setting the peak fraction to 100%. For comparison, the size distribution of the Fcj1 complex determined in B is included as a reference (gray). The peak fractions of protein size markers are indicated by arrows.

Published June 15, 2009

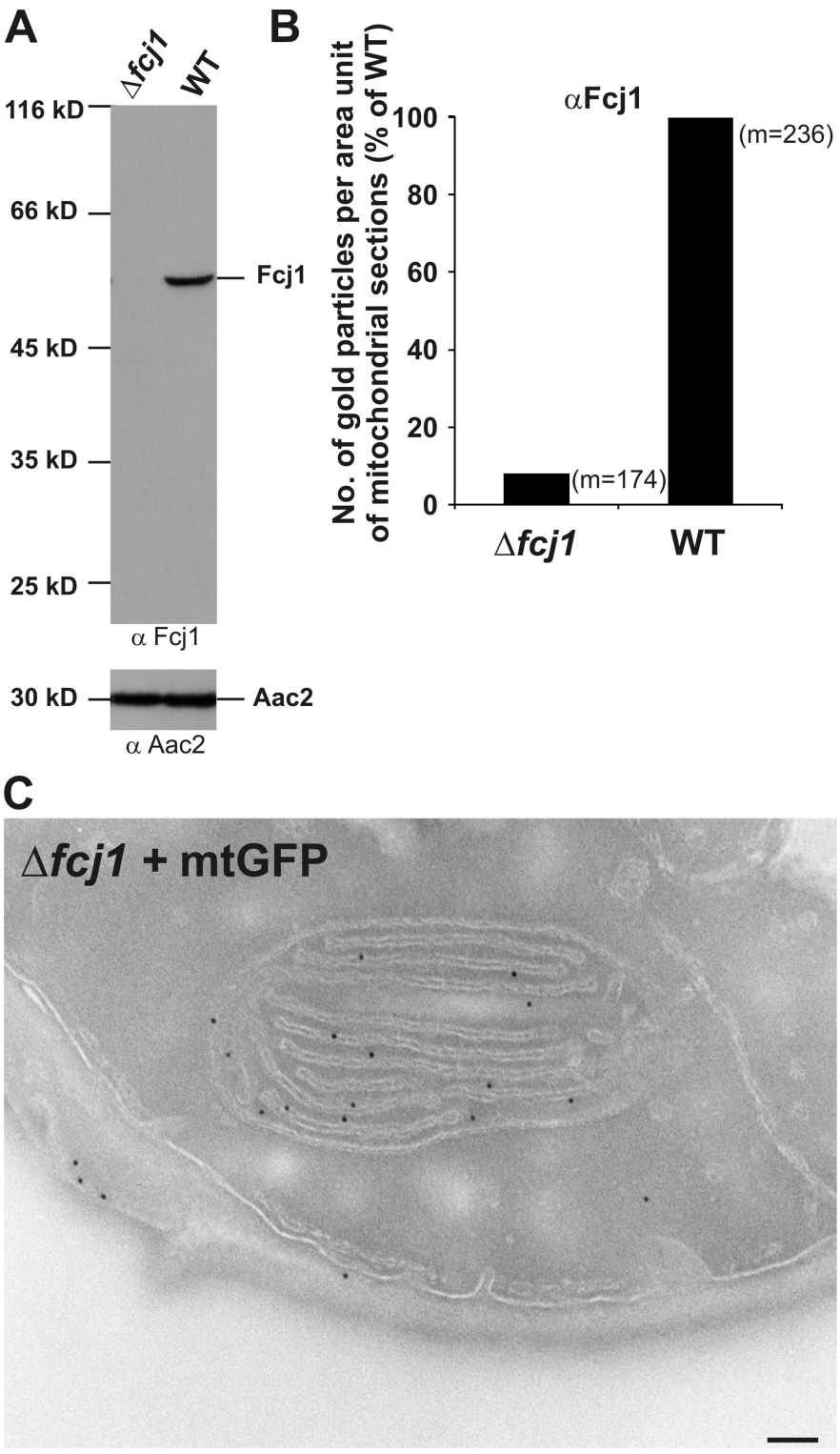


Figure S3. **Specificity of Fcj1-directed antibodies and immuno-EM in Δ*fcj1* cells.** (A) Western blotting. Equal amounts of wild-type (WT) and Δ*fcj1* mitochondria (30 µg) were analyzed by Western blotting with antibodies against Fcj1 and Aac2. (B) Quantification of immuno-EM. After immunogold labeling of Fcj1, wild-type and Δ*fcj1* cells were screened for the presence of gold particles. The number of gold particles per mitochondrial area unit in wild-type sections was set as 100%. m, number of mitochondrial sections. (C) Matrix-targeted GFP (mtFGP) was expressed in Δ*fcj1* cells and labeled with immunogold using antibodies against GFP to distinguish between the matrix and intermembrane space. The majority of gold particles appears outside and between cristae stacks, indicating that these structures enclose the intracristal space rather than the matrix space. Bar, 100 nm.

Published June 15, 2009

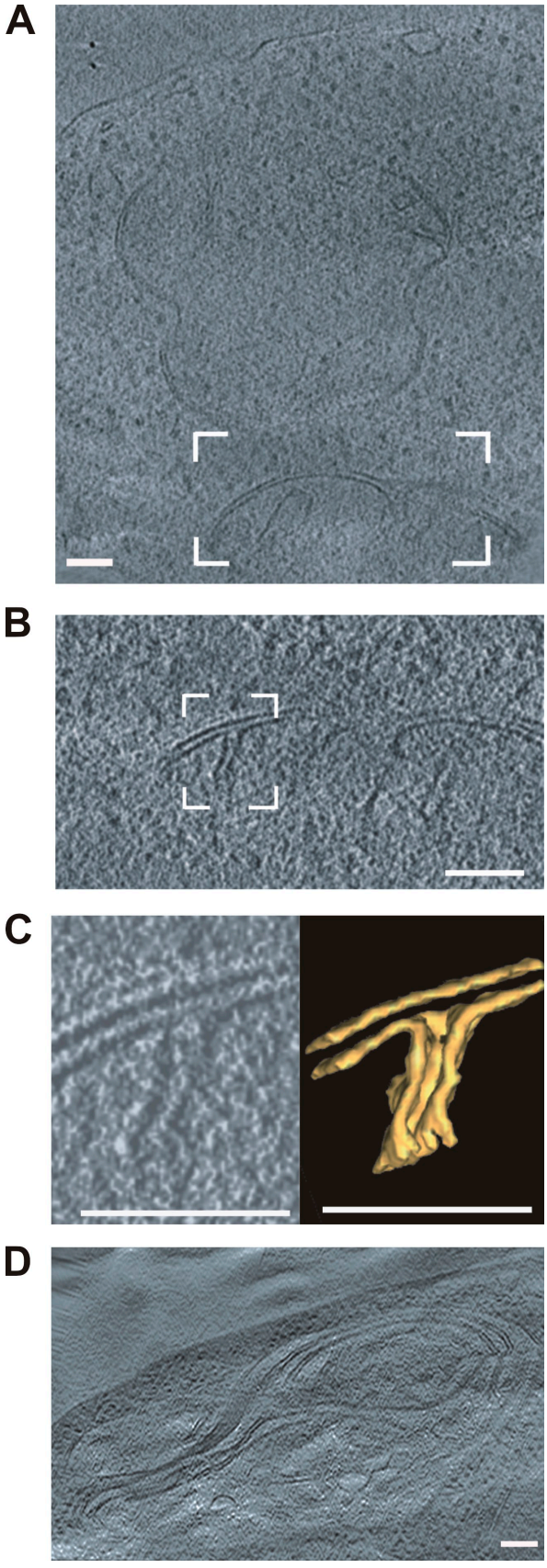


Figure S4. **Deletion of Fcj1 leads to altered cristae morphology.** (A–D) Cryo-EM tomograms of cryohydrated sections of spheroplasted yeast cells. (A) Wild-type yeast cell with two cryosectioned mitochondria. (B) CJ of wild-type mitochondrion magnified from the boxed area in A. (C) An enlargement of the boxed area in B (left) and a surface-rendered view (right) are shown. (D) Δ*fcj1* cell with cryosectioned mitochondrion showing cristae stacks. Bars, 100 nm.

Published June 15, 2009

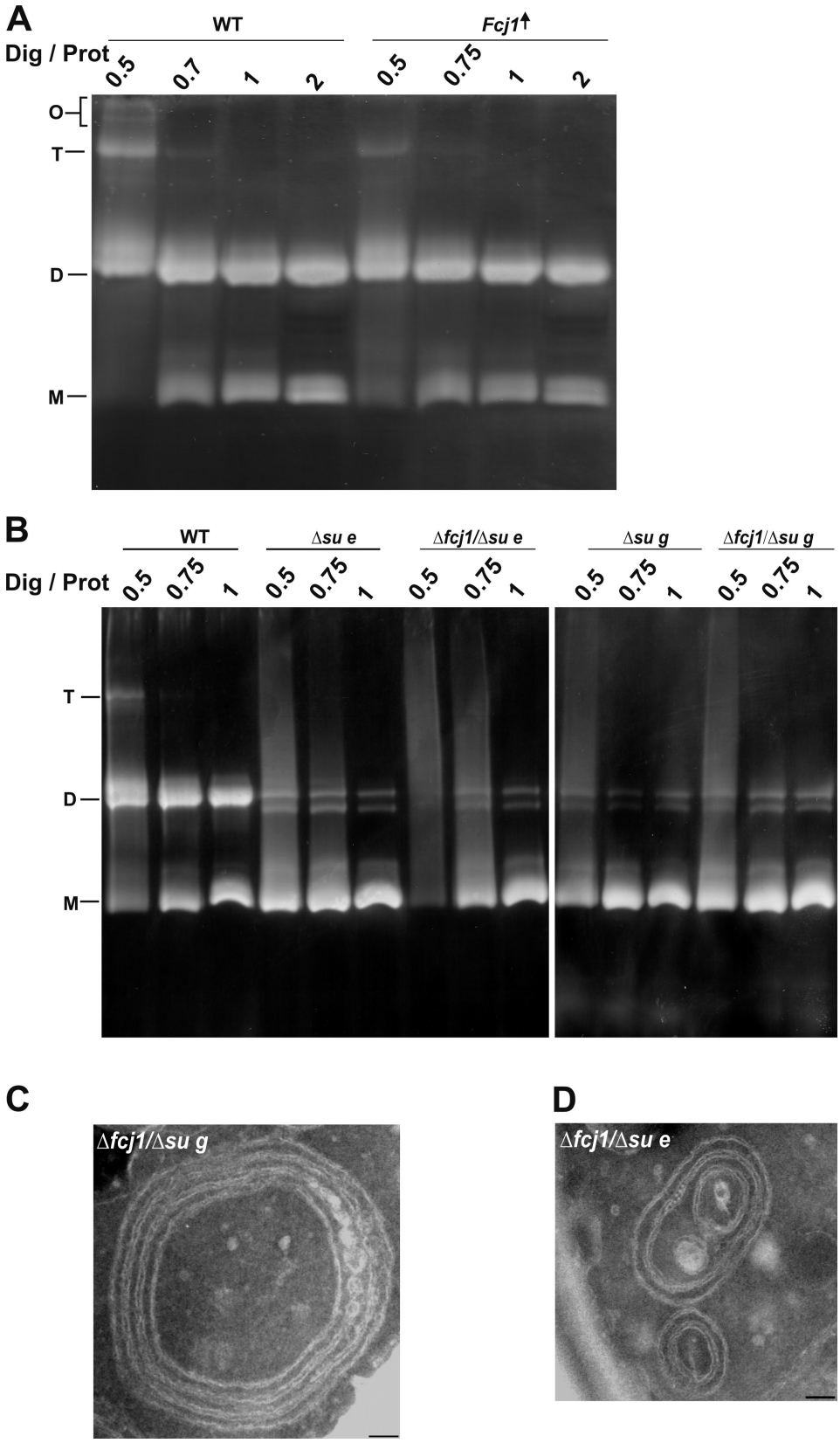


Figure S5. **Analysis of double deletion strains Δ*fcj1*/Δ*su e* and Δ*fcj1*/Δ*su g* and of a strain overexpressing Fcj1.** (A and B) Equal amounts (400 µg) of wild-type (WT) and Fcj1-overexpressing mitochondria (Fcj1↑; A) or of wild-type, Δ*su e*, Δ*fcj1*/Δ*su e*, Δ*su g*, and Δ*fcj1*/Δ*su g* mitochondria (B) were solubilized at the indicated ratios of digitonin/protein (Dig/Prot; g/g) and analyzed by BN-PAGE and by in-gel $F_1F_O$–ATPase activity. (C and D) Electron micrographs of Δ*fcj1*/Δ*su g* (C) and Δ*fcj1*/Δ*su e* (D) mitochondria in chemically fixed yeast cells. Cells were cultivated on a nonfermentable carbon source before fixation. Bars, 100 nm.

Published June 15, 2009

Table S1. **Quantitative analysis of wild-type and Δ*fcj1* cells**

| Stereological parameter used for comparison | Wild type | Δ*fcj1* |
|---|---|---|
| Ratio of membrane length IM/OM | 1.57 ± 0.25 (m = 5) | 3.29 ± 0.64 (m = 12) |
| Ratio of mitochondrial volume/cell volume | 0.21 ± 0.06 (m = 16) | 0.26 ± 0.08 (m = 17) |
| Ratio of mitochondrial area per mitochondrion relative to wild type | 1 (m = 38) | 2.0 (m = 31) |

m, number of mitochondria or mitochondrial sections. Electron micrographs of the indicated cells after chemical fixation (Tokuyasu method) were analyzed by standard stereological tools (Griffiths, G. 1993. Fine Structure Immunocytochemistry. Springer-Verlag, Berlin. 459 pp.) for membrane length and the mitochondrial area per section. The assessment of mitochondrial volumes was performed by analyzing images obtained after confocal fluorescence microscopy of strains expressing mitochondrial GFP (see Materials and methods). Mean values ± standard deviations are given.

Table S2. **Strains**

| Name | Description | Background/ genotype | Plasmids | Source |
|---|---|---|---|---|
| BY4741 | WT | BY4741 | NA | EUROSCARF |
| Δ*fcj1* | Δ*fcj1* | BY4741 | NA | EUROSCARF |
| Δ*su e* | Δ*su e* | BY4742 | NA | Open Biosystems |
| Δ*su g* | Δ*su g* | BY4742 | NA | Open Biosystems |
| Δ*fcj1*/Δ*su e* | Δ*fcj1*/Δ*su e* | BY4742 | NA | This study |
| Δ*fcj1*/Δ*su g* | Δ*fcj1*/Δ*su g* | BY4742 | NA | This study |
| *Fcj1-TAP* | *Fcj1-TAP* | BY4741 | NA | Open Biosystems |
| *Fcj1-His*$_6$ | *Fcj1-His*$_6$ | W303 | pYX242–Fcj1-His$_6$ | This study |
| *Fcj1-His*$_{12}$ | *Fcj1-His*$_{12}$ | W303 | pYX242–Fcj1-His$_{12}$ | This study |
| *Fcj1-TAP/Fcj1-His* | *Fcj1-TAP/Fcj1-His*$_6$ | BY4741 | pYX242–Fcj1-His$_6$ | This study |
| Δ*Fcj1 + pCM189-Fcj1* | Fcj1↓ used for down-regulation experiments | W303 | pCM189-Fcj1 | This study |
| WT + pCM189 | WT control strain for overexpression/ down-regulation experiments | W303 | pCM189 | This study |
| WT + *pCM189-Fcj1* | Fcj1↑ overexpression experiments | W303 | pCM189-Fcj1 | This study |

EUROSCARF, European *Saccharomyces Cerevisiae* Archive for Functional Analysis; NA, not applicable; WT, wild type.

Table S3. **Plasmids**

| Name | Description | Vector | Source |
|---|---|---|---|
| pYX242 | Yeast expression vector containing constitutive *TPI* promoter | NA | EMD |
| pCM189 | Yeast expression vector containing doxycycline-regulatable promoter system | NA | Garí et al., 1997 |
| pVT100U-mtGFP | Expression of mitochondrial matrix-targeted GFP | NA | Westermann and Neupert, 2000 |
| pCM189-Fcj1 | Expression of Fcj1 under a doxycycline-repressible promoter | pCM189 | This study |
| pYX242–Fcj1-His$_6$ | Expression of C-terminally His-tagged Fcj1 | pYX242 | This study |
| pYX242–Fcj1-His$_{12}$ | Expression of C-terminally His-tagged Fcj1 | pYX242 | This study |

mtGFP, mitochondrial GFP; NA, not applicable.

## References

Garí, E, L. Piedrafita, M. Aldea, and E. Herrero. 1997. A set of vectors with a tetracycline-regulatable promoter system for modulated gene expression in *Saccharomyces cerevisiae*. *Yeast*. 13:837–848.

Westermann, B., and W. Neupert. 2000. Mitochondria-targeted green fluorescent proteins: convenient tools for the study of organelle biogenesis in *Saccharomyces cerevisiae*. *Yeast*. 16:1421–1427.

Table S4. **Oligonucleotides**

| Name | Sequence |
|---|---|
| Fcj1 forward | 5′-CCCCCCATGGCAATGCGAAGAACTACTGCCTCACG-3′ |
| Overexpression Fcj1 reverse | 5′-CCCCGCGGCCGCTCACAACGTCCTTATTTCACAGTCTTC-3′ |
| Fcj1-His$_6$ reverse | 5′-CCCCCTCGAGTCAGTGATGGTGATGGTGATGCAACGTCCTTATTTCACAGTCTTC-3′ |
| Fcj1-His$_{12}$ reverse | 5′-CCCCCTCGAGTCAGTGATGGTGATGGTGATGGTGATGGTGATGCAACGTCCTTATTTCACAGTCTTC-3′ |
| Fcj1-HIS3 upstream | 5′-AAAGGCATAAGAACGCATTGAAAAGTCTAAAAAACTAATATTCGTCGTACGCTGCAGGTCGAC-3′ |
| Fcj1-HIS3 reverse | 5′-TTGAGGTGTAATGACGTACATCTCTTTTCTCTTTGTATTATTCTTATCGATGAATTCGAGCTC-3′ |
| Fcj1 upstream | 5′-GGTAATTTTCTTGCATTTCC-3′ |
| Fcj1 downstream | 5′-TCTTCTTTATTAAAGCCTCC-3′ |

Published June 15, 2009

Video 1. **EM tomogram of chemically fixed wild-type *S. cerevisiae* cell.** Successive xy slices through the tomogram are shown moving along the tomographic z axis. The top right mitochondrion was used for surface rendering and is shown in Fig. 3 (A and B). The video is shown at 30 frames/s.

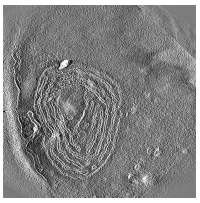

Video 2. **EM tomogram of chemically fixed Δ*fcj1 S. cerevisiae* cell.** Successive xy slices through the tomogram are shown moving along the tomographic z axis. A single slice of mitochondrion was used for surface rendering and is shown in Fig. 3 (C and D). The video is shown at 30 frames/s.

Video 3. **Cryo-EM tomogram of isolated wild-type *S. cerevisiae* mitochondrion.** Successive xy slices through a tomogram represented in Fig. 4 A are shown moving along the tomographic z axis. The video is shown at 30 frames/s.

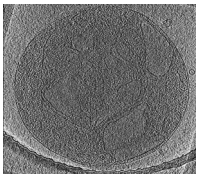

Video 4. **Cryo-EM tomogram of isolated Δ*fcj1 S. cerevisiae* mitochondrion.** Successive xy slices through a tomogram represented in Fig. 4 C are shown moving along the tomographic z axis. Details are shown in Figs. 4 (D–G) and 5 B. See also Video 5. Zipperlike structures typical of the $F_1$ parts of $F_1F_O$–ATP synthases are visible. The video is shown at 30 frames/s.

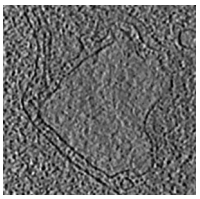

Video 5. **Cryo-EM tomogram of isolated Δ*fcj1 S. cerevisiae* mitochondrion.** Successive xy slices through a tomogram represented in Fig. 4 D are shown moving along the tomographic z axis. This represents an enlargement slightly below the boxed area in Fig. 4 C. Zipperlike structures typical of the $F_1$ parts of $F_1F_O$–ATP synthases are visible. The video is shown at 30 frames/s.